UNIVERSITÀ DEGLI STUDI DI MILANO
DEPARTMENT OF COMPUTER SCIENCE

COMPUTER SCIENCE PH.D. PROGRAM

DEVELOPMENT AND APPLICATION OF SEGMENTATION AND ANALYSIS METHODS FOR THE MORPHOLOGICAL AND FUNCTIONAL CHARACTERIZATION OF THE LOWER LIMB FROM MRI IMAGES

Advisor: Prof. Nunzio Alberto Borghese
Coadvisor: Ing. Giovanna Rizzo
Coordinator: Prof. Paolo Boldi

Doctoral dissertation of:
Orgiu Sara
Matr. Nr. R10621

XXIX Ph.D. cycle
anno accademico 2016-2017

Abstract

This work is aimed to the development and application of a segmentation and analysis methods for the morphological and functional characterization of the lower limb from MRI images.

Regarding the morphological characterization, an automatic algorithm was developed for the segmentation of Skeletal Muscle (SM), Intermuscular Adipose Tissue (IMAT), and Subcutaneus Adipose Tissue (SAT) compartments from cross-sectional T1-W MRI images [1], in order to assess thigh regional tissue composition in both young and elderly subjects with different degrees of body adiposity, including obese individuals. A fuzzy c-mean algorithm was employed to perform a classification of the different tissues: SM, Adipose Tissue (AT) and bone. Muscle fascia, which is the anatomical structure that separates SAT and IMAT compartments, was segmented using a procedure based on Snake active contour model.

We validated the segmentation framework on 15 datasets from 5 young normal weight, 5 older normal weight and 5 older obese females using manual segmentations delineated by an expert operator as gold standard. Segmentation errors were assessed for each structure resulting in mean relative area difference of 1.8%, 2.5% and 2.7% for SM, bone and AT, respectively, and a mean sensitivity for each compartment above 96% in each subject typology. Muscle fascia identification performance resulted in a mean distance between manual and automatic contours of 0.81mm and a mean percentage of contour pixels with distance smaller than 2 pixels of 86.2%. Moreover, manual and automatic IMAT and SAT cross-sectional areas in all subject typologies were found significantly correlated ($p < 0.001$). These results indicate that the proposed automatic segmentation algorithm, adequately performing thigh tissue discrimination, could be an helpful tool in studies of thigh regional composition. To our knowledge, this is the first published approach which identifies muscle fascia in its anatomical position obtaining promising results from a low level based segmentation perspective.

Regarding the functional characterization of the lower limb, the properties of a specific region of the SM: the quadriceps femoris was considered representative of the entire compartment. In this region, size and fat content of 6 normal weight and 5 obese well functioning older females were determined at mid-thigh of the dominant

leg, by analysing MRI Dixon images. These data as well as peak knee-extension torque, muscle fascicle length and pennation angle were compared in order to assess functional differences between the two groups. The study [2] showed that muscle tissue composition and pennation angle are important determinants of muscle torque per unit muscle section in well-functioning older women. Moreover, as a result of the greater gravitational load, active obese elderly women have more muscle mass but with a higher fat content compared with normal-weight counterparts.

The amount and distribution of SM and AT in different body regions, have a relevant clinical impact. In particular, the assessment of changes in both SM and AT amount and distribution are significant as they correlate with processes related to aging. Namely, a loss of SM mass with an increasing of IMAT have been identified as a negative correlate of SM quality and strength in lower limb, leading to functional impairment of different severity. Moreover, the simultaneous presence of such conditions with an abnormal high accumulation of AT in the lower limb has been defined as sarcopenic obesity and correlated with accelerated functional decline with high risk of diseases and mortality.

This work represents a step forward not only to the accomplishment of accurate patient-specific thigh tissues segmentation and quantification, but also to the understanding of processes related to aging with the concomitant presence of obesity.

Contents

List of Figures

List of Tables

List of Abbreviations

ASD Average Symmetric Distance

AT Adipose Tissue

BMI Body Mass Index

CSA Cross Sectional Area

CT Computer Tomography

D-SE Disk shaped Structuring Element

DTI Diffusion Tensor Imaging

EMG ElectroMyoGraphy

FN False Negative

FL Fascicle Length

FP False Positive

HU Hounsfield Unit

IP In Phase

IPAQ International Physical Activity Questionnaire

IMAT Intermuscular Adipose Tissue

LEMS Local Entropy Minimization with a bicubic Spline model

Less 2 Pixels Percentage of contour pixels with distance from the reference contour smaller than 2 Pixels

mfMRI muscle functional Magnetic Resonance Imaging

MF Percentage of fat content of quadriceps femoris

MRI Magnetic Resonance Imaging

MRS Magnetic Resonance Spectroscopy

NW Normal Weight

OB Obese

O-NW Older Normal Weight

O-OB Older Obese

OP Out of Phase

PA Pennation Angle

KET Knee Extension Torque

PCSA Physiological Cross-Sectional Area

QF Quadriceps Femoris

R Radius

RAD Relative Area Difference

RF Rectus Femoris

SM Skeletal Muscle

SAT Subcutaneous Adipose Tissue

SNR Signal to Noise Ratio

T1-W MRI T1-Weighted Magnetic Resonance Imaging

TN True Negative

TP True Positive

US Ultrasound

VI Vastus Intermedius

VL Vastus Lateralis

VM Vastus Medialis

Y-NW Young Normal Weight

Chapter 1

Introduction

1.1 Motivation

The amount and distribution of Skeletal Muscle (SM) tissue and Adipose Tissue (AT) in different body regions, have a relevant clinical impact. In particular, the quantification of SM in the lower limb plays a crucial role in the diagnosis and treatment of neuromuscular diseases [4] as well as being a reliable index for evaluating the success of therapies aimed to reduce the progression of pathological conditions involving muscle atrophy [5]. Moreover, a precise estimation of muscle mass is fundamental in studies of exercise physiology to obtain reliable estimation of muscle performance in terms of strength and functionality [6].

The distribution of lower limb AT has been found correlated with the development of metabolic abnormalities. In particular, the Intermuscular Adipose Tissue (IMAT), located beneath the fascia lata within and adjacent to SM, has been recognized as an important prognostic factor for insulin sensitivity and cardiovascular risk [7, 8, 9] .

In addition, the assessment of changes in both SM and AT amount and distribution are significant as they correlate with processes related to aging. Namely, a loss of SM mass with an increasing of IMAT has been identified as a negative correlate of SM quality and strength in lower limb, leading to functional impairment of different severity [10].

Moreover, the simultaneous presence of such conditions (Sarcopenia) with an abnormal high accumulation of AT in the lower limb has been defined as sarcopenic obesity and correlated with accelerated functional decline with high risk of diseases and mortality [11].

The tissue morphological characterization, alone, is not sufficient to understand the pathways by which obesity affects physical functioning in older subjects. Indeed, Obese (OB) individuals demonstrate more SM and higher muscle strength [12]. However, the strength normalized for body weight results lower in OB than in non-OB

adults.

Magnetic Resonance Imaging (MRI) is widely used in clinical practice because of its property of well distinguishing between different types of soft tissues with high resolution and non-invasivity. In particular, T1-Weighted Magnetic Resonance Imaging (T1-W MRI) has been recognized as the most effective technique for the study of body composition and in particular for the assessment of SM and AT distribution and quantification in different body regions [13, 14, 15, 16]. Thus, it is expected to have a substantial impact on the detection and follow-up of sarcopenic conditions. The discrimination of the different tissue compartments of interest, including SM, Subcutaneous Adipose Tissue (SAT), and IMAT and their quantification through segmentation processes, is essential to accurately assess tissue composition from MRI images. In clinical practice, this segmentation is currently performed by manually tracing the contour of all the structures of interest on each slice of the MRI data. As a standard MRI study consists of dozens of images, this procedure is time consuming and it is prone to inter and intra-operator variability. Therefore, tools capable of automatically extract the regions of interest from T1-W MRI thigh images are strongly demanded.

Dixon MRI sequence [17], relying on the water/fat chemical shift difference allows to achieve the water/fat signal separation through postprocessing. It is then possible to assess the portion of fat present in the SM. This could be an important contribution to the functional characterization of the SM. Indeed, fat infiltration in SM tissue has been found correlated to poorer isokinetic SM strenght [18].

Nowadays, thanks to these imaging techniques is thus possible to deeply investigate physiological and pathological processes such as aging and metabolic disorders. The understanding of these processes is of absolute relevance as life expectancy among the elderly has been improving for many decades with a very high impact on total health care spending [19]. In fact, it has been shown that medical costs grown with age and the population will become increasingly aged over time. However, health among the elderly is expected to moderate the increases in medical costs, improving the quality of life of elderly people [20]. In this scenario, the early detection and an accurate follow up of morphological and functional changes in the musculoskeletal system correlated to disorders and pathological conditions is fundamental. As the amount and distribution of SM and AT in the thigh have been found strictly correlated with cardiovascular risk and metabolic disorders, and thigh muscles are essential for gait and physical normal functioning, we concentrated our work on the morphological and functional characterization of this specific region in order to provide clinicians a valid support on the understanding and quantification of changes in regional composition related to metabolic processes characterizing aging.

1.2 Aim and Contributions

The object of this thesis is the development, validation and application of clinically feasible strategies for the morphological and functional characterization of the lower limb from MRI images acquired with different sequences in subjects with different characteristics in terms of SM and AT distribution. In particular, we have developed new tools, aiming at supporting the segmentation and analysis of data coming from images in studies of regional tissue composition and on the thigh particularly.

This work makes the following contributions:

- Thigh Tissues Segmentation: an automatic segmentation framework able to extract SM, IMAT, and SAT from T1-W MRI of the thigh. For this purpose, a fuzzy C-mean classification with active contour snake was proposed. We evaluated the method on young and older women with different degrees of body adiposity.

  An accurate automatic segmentation method is essential for the patient specific morphological characterization of the thigh, including the quantification of the different tissues of interest. Currently, no fully automatic and robust solutions are commercially available and clinicians perform segmentation manually. This practice, highly time consuming, is unfeasible for a large cohort of patients. Several works have been proposed to address thigh segmentation, but especially the identification of the weak edge of muscle fascia which separates SAT and IMAT is still an open issue. A detailed description of the issues related to thigh segmentation, the state of art in this field and how our algorithm overcomes the limitation of previous works is presented on Chapter 3.

- A study of the effects of muscle composition and architecture on specific strength in OB older women. This SM functional characterization was performed by measuring the peak Knee Extension Torque (KET), in isometric and isokinetic conditions, the Mid-thigh Quadriceps Femoris (QF) Cross Sectional Area (CSA) and muscle tissue fat content from MRI images, muscle Fascicle Length (FL) and Pennation Angle (PA) for each muscle belly of the QF from Ultrasound (US) images.

  This study had the aim to investigate how obesity affects strength production in older individuals. A deep understanding of these processes, including muscle feature changes due to obesity could be of great help for clinicians to better interpret results from interventional investigations.

1.3 Organization

The thesis is so organized: in Chapter 2 an overview of the state of art in imaging techniques used to investigate human body composition is reported. In particular MRI contrasts and applications will be described. In Chapter 3, the new automatic segmentation approach for the discrimination of SM, IMAT and SAT is presented and validated against manual segmentations. The research concerning this chapter has been published in one journal [1] and in one conference proceedings [21]. In chapter 4, the study on the effect of SM composition and architecture on specific strength in OB older women is described. The research concerning this chapter has been published in one journal [2] and in two conference proceedings [22, 23]. Finally, in Chapter 5 results obtained in this work are summed-up and future improvements are also examined.

Chapter 2

State of Art In Human musculo-skeletal imaging

Studies of body composition in humans are usually aimed at assessing deficiencies or excesses of certain components which are linked to health risks and the development of certain diseases. Several aspects of body composition, in particular the amount and distribution of AT and the amount and composition of SM have a relevant clinical impact on the study of processes related to aging and metabolic abnormalities. Their measurement is increasingly considered in clinical practice thanks to the wide availability of muskuloskeletal imaging techniques which allow to accurately investigate these aspects with high spatial resolution. Moreover, thanks to the constant development of new imaging techniques, it is today possible to acquire SM images with information content reflecting muscle functionality.

In this chapter we will give an overview of the main techniques involved on musculoskeletal imaging.

2.1 Introduction

Imaging techniques have assumed increasing importance in the study of musculoskeletal system and in particular for the study of body composition and muscular physiology and functionality. These techniques include Computer Tomography (CT), US, and MRI. Both MRI and US are radiation-free approaches and therefore totally non-invasive. US is a real-time methodology and dynamic features of a muscle can be investigated. MRI, being a 3D technique, allows for better imaging of deep structures and by applying different sequences, different contrasts can be obtained so that different kind of images can be acquired of the same specific tissue. Both MRI and US are more commonly used than CT scanning. CT scans can detect AT infiltration and SM atrophy, characteristic of aging and metabolic disorders, with a very high

spatial resolution. However, CT scan exposes the subjects to ionizing radiation without advantage over MRI or US in terms of evaluation of muscular properties. In the next section, the operating principles of these three techniques are briefly reported. Then, based on the information typology the different protocols can provide three class of methodologies will be described:

- Methods evaluating body or regional composition and the specific dimension of the investigated muscles
- Methods evaluating muscle composition and intramuscular fat content
- Methods evaluating muscle architecture
- Methods evaluating muscle activity

2.2 Operating Principle of imaging techniques

2.2.1 CT

CT [24] is a computerized x-ray imaging procedure where the subject is irradiated typically by a cone beam of x-rays which quickly rotates around the volume to be imaged, and a system of flat panel detectors intercepts the X-ray beam passing through the imaged volume. The signal is processed through adequate algorithm (e.g Feldkamp algorithm for cone beam [25]) to reconstruct cross-sectional images of the imaged volume. CT images represent the distribution of the attenuation coefficient of X-ray in the volume imaged in a predefined section. This attenuation coefficient is highly correlated to the density of the tissue composing the imaged volume. CT is a quantitative technique, as the image pixel value are expressed in a scale related to radiodensity of distilled water: the Hounsfield Unit (HU):

$$\mu(HU) = \frac{\mu - \mu H_2O}{\mu H_2O} \times 1000$$

Therefore, soft tissues with attenuation similar to water have pixels values around zero; cortical bone has high positive values and air assumes values near -1000.

2.2.2 US

US technique [26] is a very common and widespread musculoskeletal imaging technique. This technique consists in sending a pulse of ultrasounds into the volume to be imaged and waiting for an echo to return. These returning echoes, produced by

tissue interfaces, are then elaborated to produce an image of internal structures. Ultrasounds can be described as longitudinal mechanical waves which cause particles to oscillate back and forth and produce a series of compressions and rarefactions. These waves propagate through a medium with a velocity dependent on the medium density and acoustic impedance. As the velocity of ultrasounds is considered constant in soft tissues, the time between emitting a pulse and receiving an echo is used to determine the depth of the interface. On the other hand, the amplitude of the receiving echoes gives an indication of the difference of the acoustic impedance between the interfaces.

2.2.3 MRI

MRI technique [27] is based on the interaction between protons nuclei of hydrogen atoms and magnetic fields. Once inside the powerful magnetic field produced by the MRI scanner, the proton magnetic moments tend to align with this magnetic field. With the use of radiofrequency signals, the aligned protons are pulsed and some of them absorb this energy and flip. When the radiofrequency field is switched off, the protons release the energy and tend to realign with the more powerful magnetic field generated by the MRI scanner. MRI images are obtained by analyzing the spectrum of the signal related to the absorption and emission of energy. Many kinds of contrasts can be obtained with MRI technique by varying the excitation sequences. The signal spacial localization is obtained by exciting the volume with radiofrequency pulse variations in the phase and frequency.

2.3 Body or regional composition or the specific dimension of the investigated muscles

This class of methods aims at distinguishing the different tissues of interest and in particular the AT from SM and are used for their correspondent amount estimation. The main methodologies used in this field are T1-W MRI and CT.

2.3.1 CT

CT imaging has been widely used in the past in the field of body composition and in particular for the assessment of AT and SM [13, 28], but in the last years has largely been replaced by MRI. CT is easy to apply and is characterized by small acquisition time allowing a good and standardized assessment of the morphological characterization of the tissues of interest as well as shape and size changes. Despite the very high resolution that can be obtained, CT images present a limited contrast between soft tissues of different types; this makes automatic segmentation processes

less effective. Finally, the fact that CT exams imply a high ionizing radiation exposure of the subjects makes this technique not safe, especially for repeated measurements. An example of a CT image is reported on Fig.2.1

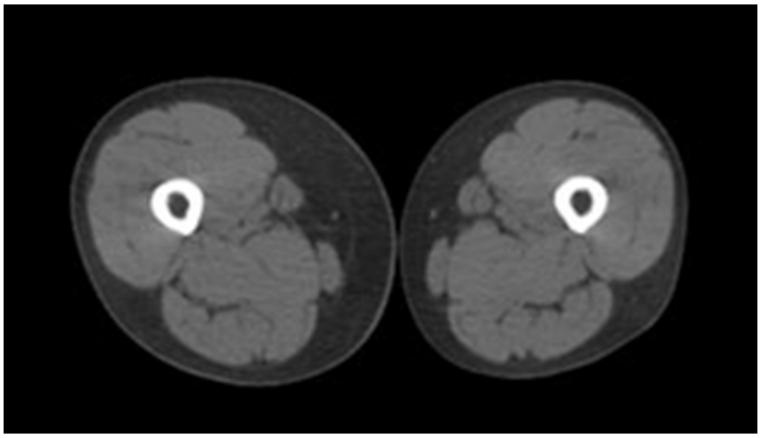

Figure 2.1: An example of CT image of the thighs.

2.3.2 T1-W MRI

T1-W MRI is one of the basic pulse sequences in MRI and the images reflect the differences in the T1 relaxation time of tissues. This time constant represents the amount of time the protons take to realign with the magnetic field after the radiation pulse is switched off. This technique has been recognized to be the most effective in the study of body composition, as it provides a large contrast between soft tissues with high resolution [13, 28]. An example of a T1-W MRI image is reported on Fig.2.2

2.4 Muscle composition and intramuscular fat content

The amount and distribution of SM and AT are not sufficient to understand processes related to aging and metabolic disorders. Indeed, there is evidence that in this kind of processes, an increase of adipose compartments is accompanied by modifications in SM composition due to a different degree of fat infiltration in muscle tissue which leads to a deficit in muscle functionality [29, 30]. Therefore, the quantification of this degree of fat infiltration is essential. Three different techniques can be used with this aim: CT, DIXON sequence MRI and Magnetic Resonance Spectroscopy (MRS).

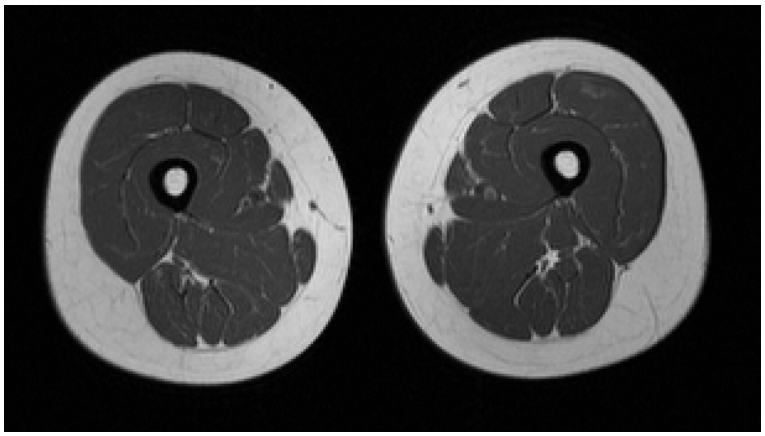

Figure 2.2: An example of T1-W MRI image of the thighs.

2.4.1 CT

CT imaging has been used in the past to assess the amount of adipose and skeletal muscle tissue and to determine the integrity of the latter [28, 29, 18, 30, 31, 32]. AT found within SM (intramuscular adipose tissue) causes a decrease in the pixels values correspondent to SM, affecting the quality of the assessment of this tissue; thus, the lower the mean HU, the lower the density and, therefore, the greater the fat content.

2.4.2 Magnetic Resonance Spectroscopy

MRS [33] is an imaging technique that allows for the noninvasive molecular characterization of a region of interest. In particular, in SM tissue MRS allows to discriminate and assess intracellular and extracellular lipid compartments as well as many other metabolites whose signals are located in a different position of the signal spectrum [34].

This technique is based on the chemical shift effect. This phenomenon consists in a slightly difference in resonance frequency for protons belonging to different molecules caused by minimal difference in the magnetic field they experience. This variability in the magnetic field is caused by the different chemical structure of molecules which determines their electronic environment. By applying specific pulse sequence, and analyzing the spectrum of the output signal, the specific amount of various metabolites can be assessed. In Fig.2.3 an example of spectrum signal obtained from a small region of the thigh acquired with MRS is reported.

This technique is very accurate and it is recognized as the gold standard for the quantification of fat [35] and in particular for discriminating intracellular and extracellular lipid compartments in SM tissue [36, 37, 38]. However, the spatial resolution of this technique is very low as large voxels are required in order to obtain

high signal to noise ratio. Many protocols foresee the acquisition of a single voxel for simplicity and to keep the acquisition time short. Multiple voxels can be also acquired in order to analyze entire compartments necessitating longer acquisition time and requiring more complex protocols to maintain a strict field homogeneity. It is also worth to note that, this protocol is not widely available in clinical practice and in order to reach the maximum accuracy it needs high magnetic fields, usually available only in research contexts.

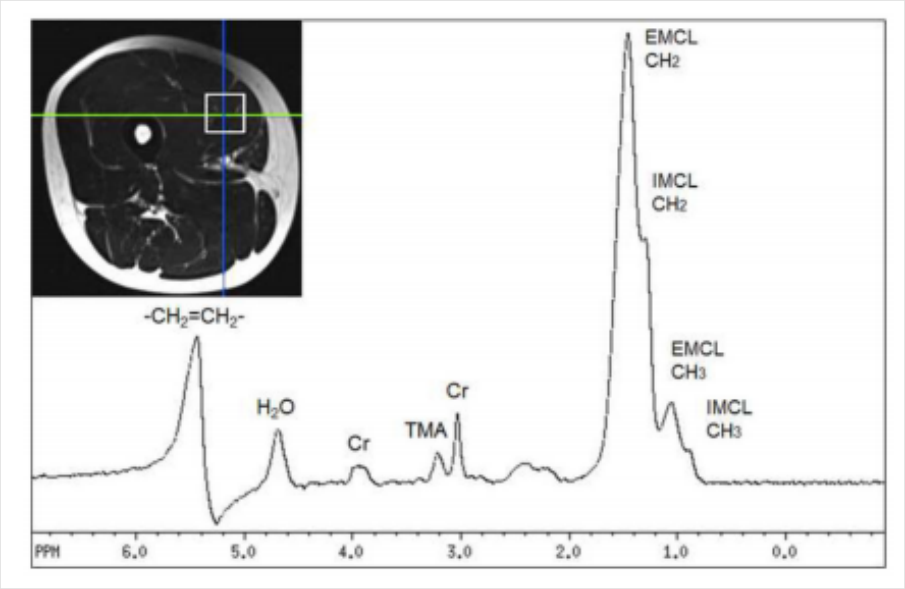

Figure 2.3: An example of the spectrum obtained with MRS from a small region of the thigh which is indicated with a white square in the anatomical image. The horizontal axis of the spectrum is labeled with frequency expressed in ppm while the vertical axes represents the amplitude of the signal. The amount of a single metabolite is strictly related to the correspondent peak amplitude. The intracellular and extracellular lipid peaks are indicated with IMCL and EMCL, respectively.

2.4.3 Dixon sequence MRI

Chemical shift encoded methods, also referred as Dixon methods [39, 40] allow to calculate the percentage of fat signal with respect to signal coming from water, by acquiring separated images of fat and water signal.

Due to different molecular properties, protons of fat and water experience different magnetic fields leading to a higher resonance frequency of water protons with respect to those of fat. Chemical shift encoded imaging exploits this difference in terms of

resonance frequency to produce In Phase (IP) and Out of Phase (OP) images. IP images, which contain the sum of the signals produced by fat and water protons, are obtained by acquiring the signal when water and fat protons are in phase coherence. On the other hand, OP images, whose pixels values represent the subtraction of the fat signal from the water signal, are obtained by acquiring the output signal when water ad fat protons are 180° out of phase.

The acquisition timing is known, as known are the resonance frequencies of fat and water protons which vary with the magnetic field amplitude. Water signal and fat signal images can be obtained by post-processing IP andOP images. The water images are calculated by performing a voxel to voxel sum of the IP and OP images, while fat images are obtained by performing a voxel to voxel subtraction of the OP image voxel values from the corresponding IP image data values.

The technique, above described, is called two-point Dixon technique [17] as two images are acquired. An example of images obtained with a 2 point Dixon protocol is shown in Fig.2.4. Dixon protocols with more sets of images have been developed in order to overcome possible artifacts which affect the images and distort the acquired signal [39, 40]. As an example, three point Dixon protocol foresees the acquisition of a third image in order to estimate the magnetic field heterogeneity and compensate for it [41].

This technique has been proved to be very affective to estimate the adipose component in soft tissues even if its accuracy and reproducibility are not enough investigated [42]. However, in the lasts years Dixon techniques have been extensively used in musculoskeletal field [43, 44, 45] as well as in many other application fields such as liver [46] and bone marrow [47] fat content investigation. Disadvantages of this technique are the high acquisition time and the fact that being a recent technique is not widely available in clinic contexts.

2.5 Muscle architecture

Muscle architecture is defined as the organization of the muscle fibers within the muscle relative to the line of force generation [48] and it has been recognized as one of major factors determining muscle functional performance. Muscle architecture is mainly described by three parameters: FL, PA and Physiological Cross-Sectional Area (PCSA) (See Appendix A). These architectural parameters are mainly measured using B-mode US and Diffusion Tensor Imaging (DTI).

2.5.1 B-mode ultrasound

US represents the standard technique to investigate muscle architecture. Thanks to this technique it is possible to investigate architectural parameters, such as PA and

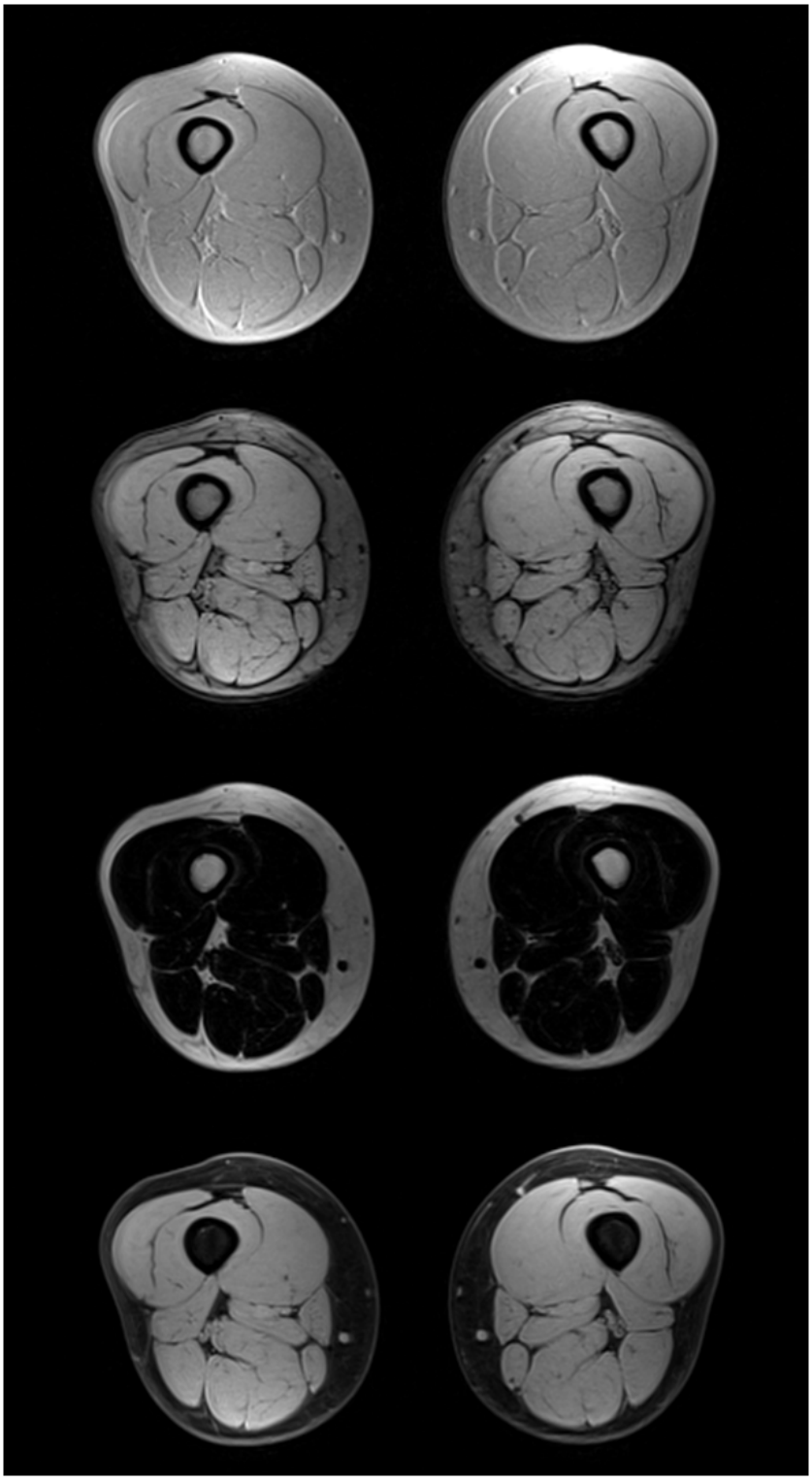

Figure 2.4: An example of images obtained with a 2 point Dixon protocol. From top to bottom we have: IP, OP, Fat and Water images, respectively.

FL, in real time. Moreover, this technique is totally non invasive and not expensive. Although the accuracy of this technique in determining muscle architectural parameters has been validated with anatomical measurements on cadavers [49], some limitations have to be considered. Firstly, US is an operator dependent approach so it is subject to reproducibility problems related to intra end inter-operator variability and distortion of the images can occur if there is too much probe pressure. In addition, the field of view is limited and the structures of interest can be imaged only partially. Finally, the US is a 2D technique, but muscle fibers are organized in 3D.

An example of muscle US image is shown in Fig.2.5

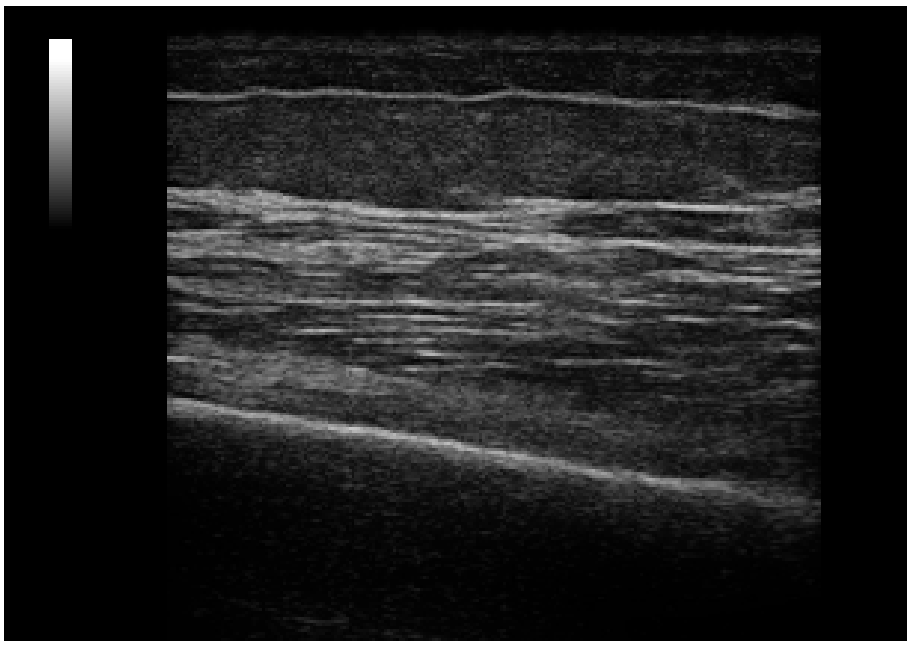

Figure 2.5: An example of a muscle US image.

2.5.2 Diffusion Tensor Imaging

DTI [50] technique allows, through specific pulse sequences, to image signal strictly related to the diffusion of water of the tissues of interest in a certain number of directions of interest to quantify the directional anisotropy of the diffusion process. Starting from this kind of signal, through a process referred as tractography, it is possible to visualize (Fig.2.6) and quantify the macroscopic muscle architecture in terms of fibre structure and arrangement. Indeed, muscle fiber tractography allows for a very accurate quantification of architectural parameters such as PA, curvature, FL, and PCSA [51, 52, 53].

An example of the result of skeletal muscle tractography is shown in Fig.2.6

A limitation of this technique resides in the fact that the presence of high infiltration of fat in the muscle can cause the tractography process to fail as fat that infiltrates muscle presents a diffusivity lower than their non-infiltrated counterpart. It has been shown that, in order to obtain an accurate tractography analysis, the region of interest should contain at least 76% of muscle tissue.

Despite the high cost of instrumentation and facilities and the complex image processing required, SM fiber tracking from DTI images is expected to give an important contribute on the study of muscle structure, becoming the reference technique for the study of parameters related to muscle architecture.

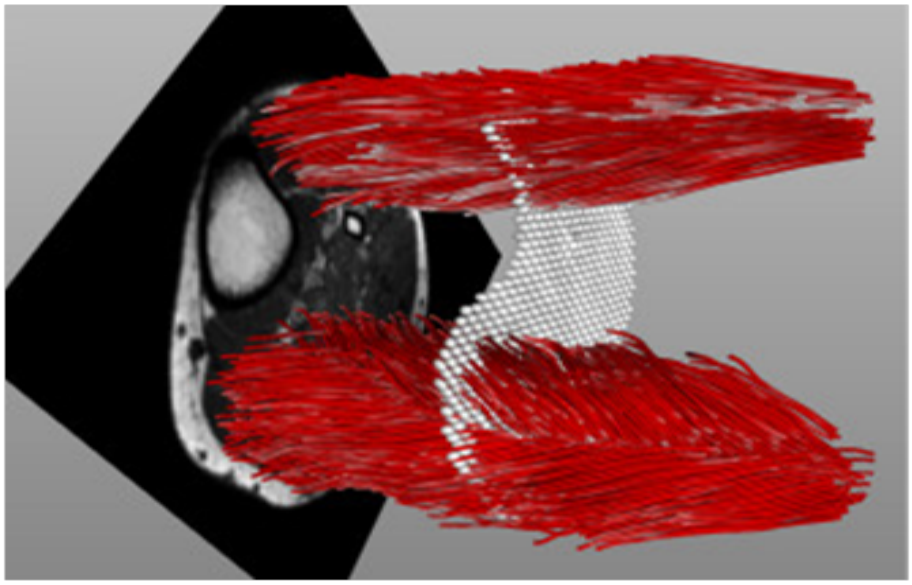

Figure 2.6: An example of a muscle tractograpy.

2.6 Muscle activation

Muscle activation is commonly measured by mean of ElectroMyoGraphy (EMG) [54] which detects the muscle's electrical activity. In the last years, the T2-mapping technique, also referred as muscle functional Magnetic Resonance Imaging (mfMRI) [55], has been found correlated with EMG signal.

2.6.1 mfMRI

It is known that exercise induces changes in the amount and distribution of water in the muscles. These changes produce a variation in the tissues of the transverse

relaxation time T2 that is a parameter of water protons that can be measured with MRI. The variation of these values have been found highly correlated with EMG signal as well as with the torque evoked by electrical stimulation. Moreover, the T2 in muscle increases with the intensity of exercise [56].

The main advantage of the use of mfMRI over EMG is that the activation can be detected on the entire muscle with an high spatial resolution allowing to fully characterize muscle activation which can reveal the real spatial distribution of activated muscle fibers during a specific task[57, 58, 59]. This kind of analysis can also be determinant on the understanding of muscle fiber recruitment patterns and how they are related to muscle function and architecture.

2.7 Discussion

Musculo-skeletal imaging had an essential role in this work as it allowed us to obtain the necessary data for our analysis. In Table2.1 the main advantages and disadvantages of the different imaging techniques used for the investigation of the musculoskeletal system are reported.

We needed high resolution anatomical images to be able to discriminate the different tissues of the thigh and in particular to detect muscle fascia which separates IMAT from SAT compartments. We adopted T1-W MRI protocol to this aim. This technique, totally non-invasive, offers a great contrast between soft tissues allowing to identify muscle fascia. This protocol is also common to all the MRI scanners and thus our automatic segmentation method could be potentially used in a wide set of clinical contexts. The alternative would have been the use of CT protocols. Despite the similar costs, we would have exposed our subjects to ionizing radiations useless. Moreover, in CT images the muscle fascia is totally invisible and so IMAT and SAT cannot be distinguished. For these reasons, CT was totally excluded from the entire protocol.

In order to investigate SM composition, a three point Dixon sequence was used in a single slice protocol. This protocol was adopted because, contrarily to MRS, Dixon sequences allow to investigate a wide muscle region with a high spatial resolution and accuracy in quantifying the fat component, while keeping the acquisition time short. A short acquisition time was absolutely required in our study as older people were involved and they were asked to stay still for all the acquisition time.

Finally, to avoid further elongation of acquisition time in MRI protocol and for economic reasons US imaging was preferred over DTI to investigate SM architectural parameters despite the lower accuracy provided by this technique.

Information Provided	Technique	Advantages	Disadvantages
Body or regional composition and muscle dimension	CT	High resolution Short acquisition time	Low contrast Ionizing radiation
	T1-W MRI	High contrast High resolution	High costs Long acquisition time
Muscle composition and intramuscular fat content	CT	Quantitative measurement High resolution	Low contrast Ionizing radiation
	MRS	High accuracy	Low resolution Complex protocols Long acquisition time
	Dixon	Effective in estimating fat content High resolution	Long acquisition time High costs
Muscle architecture	US	Sample protocols Low costs	Operator dependent Limited field of view
	DTI	High resolution High accuracy	Long acquisition time Complex protocols
Muscle activation	mfMRI	High resolution	Long acquisition time High costs

Table 2.1: Advantages and Disadvantages of the muscular imaging techniques described in this chapter.

Chapter 3

Automatic Segmentation of the thigh from T1-Weighted MRI images

Studies of regional composition are fundamental to understand and monitor processes related to age and overweight. In particular, changes on the lower limb tissue composition, such as increase on fat depots and reduction of SM, have been found correlated to muscle impairment and disability. In last years, MRI has been recognized as the most effective technique for the study of distribution and quantification of SM and AT. Manual segmentation of entire MRI datasets, aimed at discriminating the different tissues of interest, is unfeasible because the process is highly time consuming. In this context, automatic segmentation methods are a compelling need.

In this Chapter we propose an automatic method for the segmentation of SM, IMAT and SAT compartments in T1-W MRI of the thigh.

3.1 Introduction

In T1-W MRI images high contrast is visible between the AT and the muscle thanks to their different properties in terms of longitudinal magnetization recovery. However, this contrast is often significantly corrupted by intensity inhomogeneities caused by the use of surface coils necessary to investigate large fields of view. On the other hand, there is no significant intensity difference between adipose tissue belonging to IMAT and SAT compartments. IMAT compartment includes the fat tissue between muscles that is enclosed by the muscle fascia, which is a thin layer of fibrous connective tissue that as a matter of fact separates IMAT from SAT [60]. Therefore, in order to separate the different adipose compartments, it is essential an accurate segmentation of the muscle fascia. To this aim, it should be taken into account that the muscle fascia,

due to its poor water content, should be visualized as an absence of signal, but being surrounded by the high signal of AT, it is not entirely visible in the images due the to partial volume effect. Moreover, while in healthy young and Normal Weight (NW) subjects the muscle fascia is close to muscles, in elderly and OB subjects, due to a high degree of fat infiltration, it is located at a certain distance from the muscles and it is split in more layers. These features make automatic muscle fascia detection a challenging task which could be tricky in certain cases even for an expert eye.

Several works dealt with the automatic segmentation of the thigh [61, 62, 63, 64, 65, 66, 67], using different approaches; in particular some works [61, 62] were focused only on the muscle detection using a maximum a posteriori classifier and a fuzzy c-mean approach respectively. Others [63, 64] discriminated AT from muscle without taking into account the difference between SAT and IMAT relying respectively on concepts such as shaped histograms, adaptive thresholding and connectivity, and on the use of a fuzzy clustering algorithm. All these algorithms, exploited the large difference in intensity values between SM and AT. However, this high contrast is reduced in elderly and OB subjects which in general present high degree of fat infiltration in SM. This kind of images, often affected by intensity inhomogeneity artifacts can make intensity based methods less effective, leading to a misclassification of the tissues of interest. Only few of the proposed methods addressed the segmentation of IMAT and SAT and their quantification [65, 66, 67]. All of them separated IMAT from SAT relying on geometrical criteria instead of attempting to identify the anatomical position of muscle fascia. Namely, they assumed the internal SAT contour, correspondent to the muscle fascia, adherent to SM. This assumption is in general verified in healthy young and slim subjects, but leads to an incorrect adipose compartments classification in all those subjects which present an high fat infiltration degree.

Here we propose a new completely automatic segmentation method for accurately extract SM, IMAT and SAT depots from cross-sectional T1-W MRI of the thigh that overcomes the previous works limitations above discussed. Namely, we distinguished SM from AT by applying a proper correction of intensity inhomogeneity followed by an intensity classification method based on fuzzy c-mean algorithm. IMAT and SAT segmentation were performed by adopting a smart snake contour model able to evolve and converge toward the weak edge of muscle fascia. The study was validated on a dataset composed of young and elderly subjects with different degrees of body adiposity, including OB individuals.

3.2 DataSet

Our dataset was composed of eighteen voluntary females subjects with different ages and body adiposity. Namely, we had seven Young Normal Weight (Y-NW) (age: 27 ± 3, Body Mass Index (BMI): $20.3\pm1.8 kg/m^2$), five Older Normal Weight (O-NW)

(age: 73 ± 2, BMI: $24.3 \pm 1.8 kg/m^2$), and six Older Obese (O-OB) (age: 73 ± 4, BMI: $36.3 \pm 2.0 kg/m^2$) subjects. After a fully explanation regarding the nature of the protocol, each of them signed the informed consent form approved by the Institutional Review Board of San Raffaele hospital. The protocol consisted in a thigh MRI acquisition on an MRI Philips Achieva 1.5T scanner using a torso XL coil. A T1-W turbo spin echo sequence was implemented, with relaxation time = 550 msec, echo time = 15 msec, number of excitations = 4, echo train length 53, and bandwidth equal to 564kHz. The scan included the entire thigh, including the volume comprised between the anterior superior iliac spine to the tibial tuberosity. Cross-sectional images (orthogonal to the long axis of the body) were acquired with subjects in supine position. Between 57 and 68 slices were acquired for each subject, with a slice thickness of 6mm without interslice spacing, based on subject specific thigh length. The field of view was also optimized based an specific subject anatomy, leading to an in-plane spatial resolution between 0.81 and 1.28 mm with a correspondent matrix size in the range 220×220 and 352×352. An entire acquisition time varied between 11 and 14 minutes.

3.3 The Algorithm

The proposed entirely automatic segmentation method [1] was entirely implemented using the Image Processing Toolbox of MatLab v. 2011a (MathWorks, Natick, MA). For each image volume dataset, the algorithm was applied on each image slice included in the volume delimited proximally by the insertion of the gluteus maximus muscle and distally by the end of the rectus femoris muscle, which represented the anatomical volume of interest for the automatic segmentation method. The tuning of the segmentation algorithm parameters, detailed in the following paragraphs, was carried out using a training set composed of two Y-NW and one O-OB subjects (BMI: $24 kg/m^2$, $20.1 kg/m^2$, and $38.1 kg/m^2$, respectively), in order to assess the parameter values set which allowed the algorithm to reach the best segmentation performance as visually assessed by an expert in muscle imaging. Some parameter values were not fixed, yet varied automatically during the execution of the algorithm based on the BMI of the subject. The BMI, defined as the ratio between body mass and the square of body height, was automatically calculated by extracting subject height and body mass from the header of DICOM images.

A complete schema of our completely automatic segmentation method for discriminating SM, IMAT and SAT is shown in Fig.3.1. Firstly, the dataset was corrected for intensity inhomogeneities using Local Entropy Minimization with a bicubic Spline model (LEMS) algorithm (Section 3.3.1). Then, a rough tissue classification (SM, AT and background) was performed using the fuzzy c-mean algorithm (Section 3.3.2). Starting from the background component (Background mask), the bone was

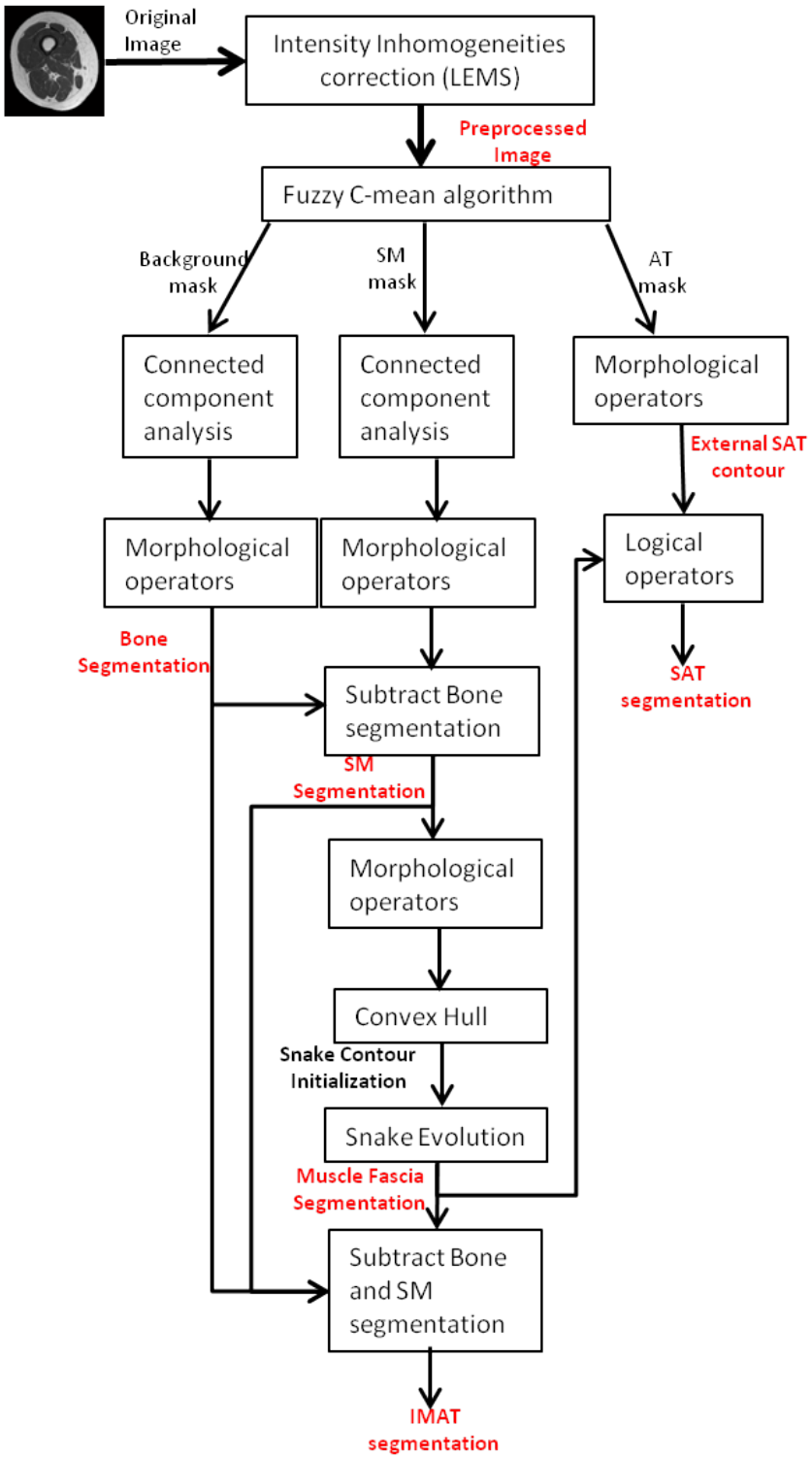

Figure 3.1: Schema of the algorithm

segmented through connected component analysis and the application of morphological operators (Section 3.3.3). SM segmentation was obtained by subtracting the bone segmentation to the SM mask processed using connected component analysis and morphological operators (Section 3.3.4). The muscle fascia was detected adopting a smart snake contour model (Section3.3.5) whose initial contour was obtained by processing the SM segmentation. IMAT was identified as the area enclosed by muscle fascia excluding SM and the bone. SAT corresponded to the filled AT mask excluding the area enclosed by muscle fascia. In the following sections the algorithm description with all details for implementation are reported.

3.3.1 Preprocessing

Intensity inhomogeneities are defined as a slow non-anatomic intensity variation of the same tissue over the image domain [68] and often affect MRI images, especially those acquired with surface coils. This artifact, if not corrected, could hindered the performance of segmentation and classification processes especially those based on intensity information. Since our segmentation approach is based only on the exploitation of low level information, before segmentation, we corrected our volumes by applying the correction algorithm LEMS [69], already successfully used with T1-W images of the calf [62].

The image signal model used is:

$$y_i = x_i b_i + n_i$$

where y_i is the intensity value of the image pixel, b_i is the bias field and n_i is the noise. The bias field is described by a bicubic spline which allows to control the smoothness, with proper spacing of the mesh defining the control points in the image, and describes accurately the intensity spatial inhomogeneity, simultaneously accounting for the eventual steep signal inhomogeneity. The bicubic spline parameters are estimated by iteratively minimizing local entropy, starting with areas with high Signal to Noise Ratio (SNR) and progressively merging neighboring areas with next highest SNR. LEMS is totally automatic and being based on entropy minimization, contrary to methods based on tissue classification, is robust and independent from initial conditions. Fig.3.2 shows an sample image and its correspondent histogram, before and after the intensity inhomogeneities correction. As can be observed, the histogram intensity peaks (SM and AT) after correction become more sharp, indicating a more homogeneous intensity distribution of the different tissues.

3.3.2 Initial Fuzzy Classification

T1-W images are characterized by a very high intensity contrast between SM and AT. Moreover, the cortical bone due to its poor water content, is characterized by

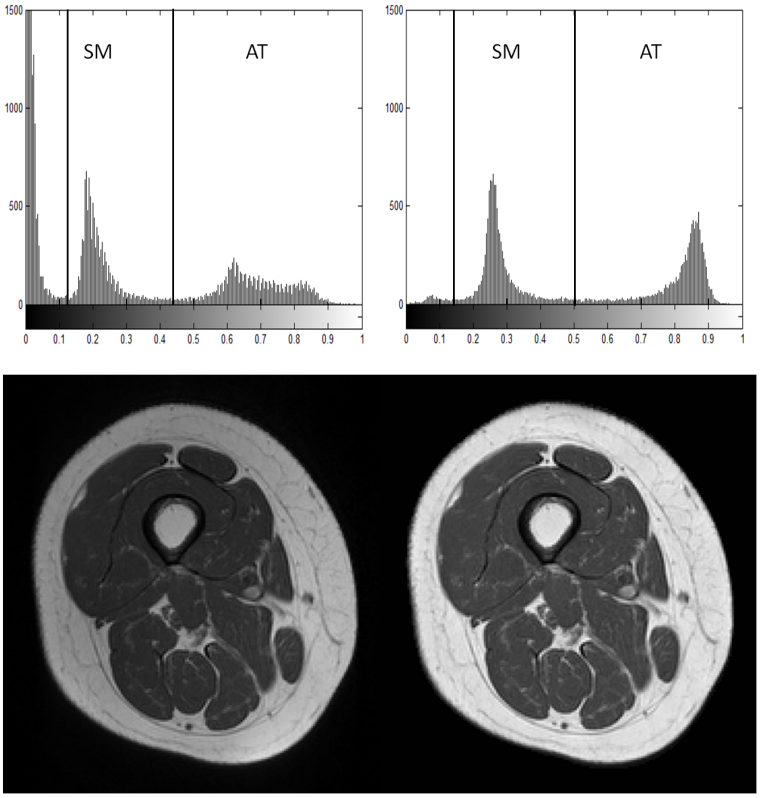

Figure 3.2: A T1-W MRI image of the thigh and its correspondent histogram before and after the application of the intensity homogeneities correction method LEMS.

the absence of signal. These properties were exploited to perform a rough initial classification of the tissues of interest by applying a standard fuzzy-c-mean algorithm [70]. The algorithm taking as input a predefined number of classes C (In this work set equal 3 as the tissues of interest are: SM, AT and Marrow bone, Sponge bone and Background), assigned to each image pixel y_i a partial membership value relative to each class j by minimizing the following cost function

$$H_{FCM} = (U, V) = \sum_{i=1}^{N} \sum_{j=1}^{C} (u_{i.j})^m \left\| y_i - v_j \right\|$$

where U is the membership function, V is the vector of class centers and m is the weighting exponent (in our case equal two) which regulates the classification fuzziness degree. The membership values associated to each pixel, for the three classes of tissue, represent the probability of the pixel to belong to the correspondent tissue. Therefore, to obtain an objective classification, a thresholding was performed to the three membership function components obtaining three different binary masks, one

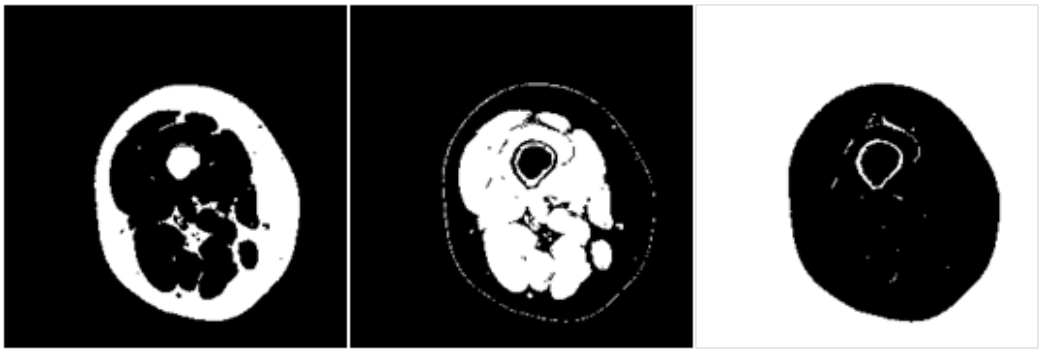

(a) (b) (c)

Figure 3.3: An example of binary masks: a) AT mask, b) SM mask, c) Background mask (which include the sponge bone).

for each tissue of interest. In particular, each pixel was set to 1 when its correspondent membership function component was greater than $0.4, 0.5$ and 0.5 for AT, SM and sponge bone-background, respectively. An example of the obtained masks is shown on Fig.3.3

3.3.3 Bone segmentation

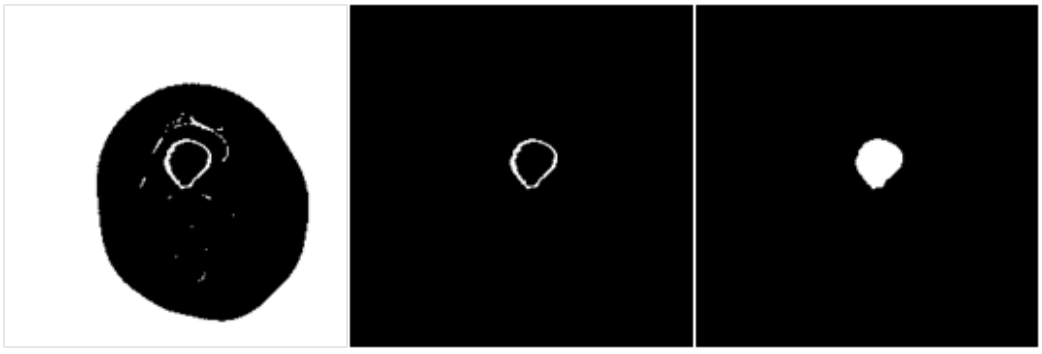

(a) (b) (c)

Figure 3.4: The bone segmentation process: a) the background mask b) the cortical bone region identified by the connected component analysis, c) the bone region segmentation.

The bone is mainly composed of two different tissues characterized by very different intensity values in T1-W MRI. In particular, as previously mentioned, the cortical

bone is characterized by an absence of signal, while marrow bone, enclosed by cortical bone, gives rise to a hyper intense signal, very similar to AT. The cortical bone was segmented by applying morphological operators to the background mask (Fig.3.4a). In particular, in this mask, a connected component analysis was performed and the cortical bone was identified as the second larger connected component (Fig.3.4b, the largest one represented the image background). Then, a morphological dilation with a Disk shaped Structuring Element (D-SE) of Radius (R) of 6 Pixels was applied to include in the segmentation very thin cortical bone areas where the pixel intensities were heavily affected by partial volume effect with the close bone marrow tissue, and thus not included in the background mask. The region enclosed by the cortical bone (correspondent to the marrow bone) was included in the segmentation with a filling process and finally a morphological erosion operation was performed with the same structuring element used for previous dilation operation (Fig.3.4c).

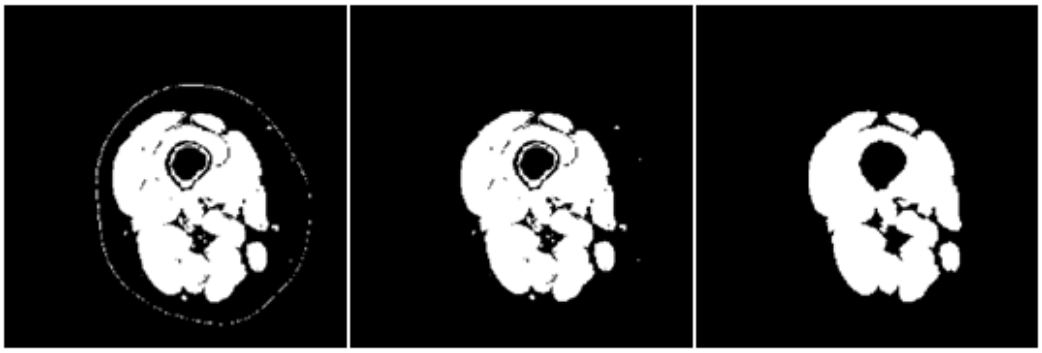

(a) (b) (c)

Figure 3.5: The SM segmentation process: a) the SM mask, b) the removal of the skin, c) the SM segmentation.

3.3.4 SM segmentation

The SM segmentation was obtained by applying morphological operator to the SM mask. In order to remove the skin, a logical AND operator was performed between the SM mask and the filled AT mask (Fig.3.5a).

Eight connected component analysis was performed, connected components with area smaller than 50 pixels were removed (typically small vessels) and small holes with area smaller than 16 pixels were filled (Fig.3.5b). Finally, a subtraction of the bone region from the obtained SM mask was performed obtaining the final SM segmentation (Fig.3.5c). A further morphological closing operation (D-SE, R=2 Pixel) was applied to OB subjects (BMI$>$ 30) in order to obtain a plausible smooth SM

segmentation. Indeed, this subject typology presented a very high SM fat infiltration, leading to an intensification of the partial volume effect which caused a tissue misclassification of the pixels located at the interface between SM and AT.

3.3.5 SAT and IMAT segmentation

The external contour of the SAT was set correspondent to the contour of the filled AT mask after a morphological closure operation (D-SE, R=2 Pixels). This last operation was executed in order to remove small irregularities, typically due to small subcutaneous vessels.

The muscle fascia which delimited SAT internally was detected through the use of an active snake evolution [71]. Starting from an initial curve $v_0(s)$ the active snake contour iteratively evolved toward a convergence curve by minimizing the following energy function:

$$E = \int_0^1 E_{int}\Big(v(s)\Big) + E_{ext}\Big(v(s)\Big)ds$$

where

$$E_{int} = \frac{\alpha|v_s(s)|^2 + \beta|v_s(s)|^2}{2}$$

and

$$E_{ext} = -\nabla I\Big(x(s)\Big)$$

E_{int} is the internal energy of the snake and reflects properties of the curve itself. Specifically α and β are the weighting parameter that control the curve tension and stiffness, respectively. E_{ext} is the External energy that is computed from the image data and drives the Snake evolution toward the contour of interest. k is its correspondent scaling factor. In our case, $I\Big(x(s)\Big)$ was a modified version of the T1-W MRI image. In particular, we created an image where all pixels not belonging to AT assumed an intensity value equal to the AT mean intensity and the AT pixels maintained intensity value correspondent to the T1-W image (Fig.3.7a). The mean AT intensity value was calculated by multiplying the T1-W image by the AT mask and then averaging all the AT intensities.This smart image preprocessing step, allowing the enhancement of the intensity contrast between AT and the muscle fascia connective tissue simultaneously reducing contrast between AT and SM, facilitated the snake evolution towards regions where muscle fascia was positioned not strictly close to SM.

A rough muscle fascia segmentation was elaborated in order to initialize the snake contour evolution. As muscle fascia enclosed SM, a morphological closing (D-SE, R= 25 Pixel) and a dilation operation (D-SE, R= 2 Pixels) were carried out to the the

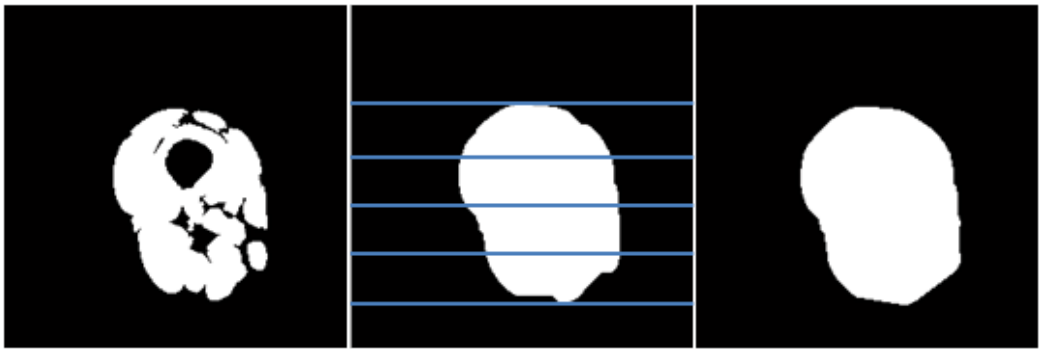

(a) (b) (c)

Figure 3.6: The snake initialization process: a) the SM segmentation mask, b) the division of the SM segmentation mask in four equal height compartments after closure and dilation operations, c) the snake initialization mask.

SM mask segmentation, obtaining a smooth compact shape positioned in proximity of the muscle fascia. Then, this area was sectioned horizontally in four equal height subareas (Fig.3.6b) and a convex hull operation was executed to the superior and inferior compartments obtaining a typical muscle fascia shaped like mask (Fig.3.6c). In OB subjects, a further morphological dilation operation (D-SE, R= 3 Pixels) was applied to the inferior compartment as this was the area where the fat infiltration was mainly concentrated and the muscle fascia tended to be located at a certain distance from SM. The contour extracted from this mask was used as the snake contour initialization $v_0(s)$ (Fig.3.7a). An example of final muscle fascia detection is shown on Fig.3.7b. The parameter values used in this work are shown in Table3.1. α, β, k were obtained by segmenting the training set with different combinations of these three parameters and visually assessing the best segmentation results. The number of iteration was set big enough to allow the active contour to reach a stable convergence. We observed that the algorithm is not sensitive to small variations of these parameters.

The IMAT compartment was obtained by subtracting from the area delimited by the segmented muscle fascia the SM and the bone areas. An example of IMAT delineation is shown of Fig.3.7c.

3.4 Segmentation Accuracy

The proposed segmentation algorithm was applied to 15 subjects: 5 Y-NW, 5 O-NW and 5 O-OB subjects composing the test set (from this set of data were excluded

Parameter	NW	OB
α	0.20	0.20
β	0.20	0.20
k	0.04	0.04
Iterations	7000	8000

Table 3.1: The parameters values used for the snake evolution.

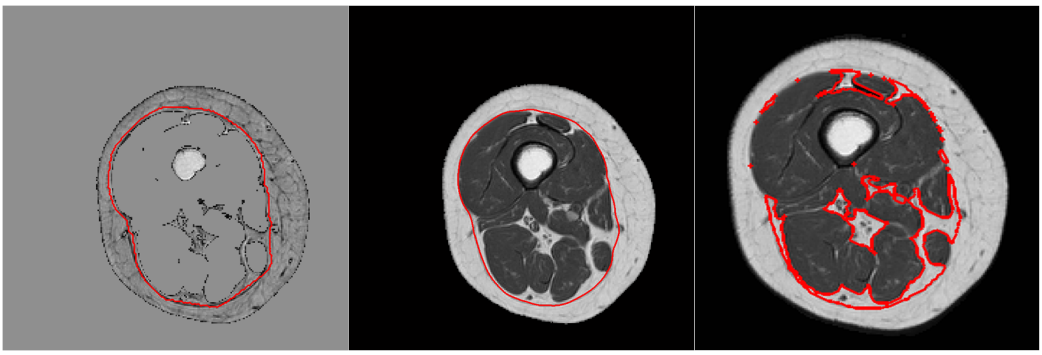

(a) (b) (c)

Figure 3.7: Muscle fascia and IMAT delineation: a) The snake initialization curve (red) superimposed to $I\Big(x(s)\Big)$, b) Convergence of the snake active contour to muscle fascia location superimposed to T1-W image c) IMAT delineation superimposed to T1-W image.

all the dataset composing the training set used in the parameter setting procedure). Based on the femoral length of the subject, between 8 and 15 equally spaced slices were extracted for each data set volume and for each slice a physiologist expert in muscular imaging manually outlined all the contours of interest (Bone, SM, Muscle fascia and external SAT contour) using the free software MIPAV 7.0.1 (http://mipav.cit.nih.gov/). These manual drawn contours were used as ground truth to estimate the algorithm accuracy in classifying the different tissues of interest (bone, SM and AT) and the accuracy of the algorithm in extracting the muscle fascia contour.

In order to evaluate the algorithm performance in classifying the tissues of interest the following accuracy indexes were calculated:

$$Sensitivity = \frac{TP}{TP+FN}$$

$$Specificity = \frac{TN}{TN+FP}$$

$$Accuracy = \frac{TN+TP}{TN+TP+FN+FP}$$

$$Precision = \frac{TP}{TP+FP}$$

Relative Area Difference (RAD) between automatic A and reference segmentation R:

$$RAD = 100\frac{|A| - |R|}{|R|}$$

where True Positive (TP) is the number of pixels correctly classified by the proposed algorithm, False Negative (FN) is the number of pixels that the algorithm erroneously excluded from tissue segmentation, False Positive (FP) is the number of pixels that the algorithm erroneously included in tissue segmentation, and True Negative (TN) is the number of pixels that the algorithm correctly excluded from tissue segmentation.

The evaluation of the algorithm accuracy in detecting muscle fascia contour for the discrimination of IMAT and SAT compartments was assessed in terms of:

Average Symmetric Distance (ASD) [72] between automatic and manual segmentation. It is defined by the following formula:

$$ASD(A, M) = \frac{1}{|C(A)| + |C(M)|}\left(\sum_{C_A \in C(A)} d(c_A, C(M)) + \sum_{C_M \in C(M)} d(c_M, C(A))\right)$$

where $C(A)$ and $C(M)$ represent all the pixels belonging to the automatically extracted contour A and the manually delineated contour M, respectively; $d(v, C(U))$ indicates the shortest distance between an arbitrary pixel and a generic contour U, calculated through the use of a 3D Euclidean distance map [73], able to detect the closest point on the test contour from each reference contour point.

Percentage of contour pixels with distance from the reference contour smaller than 2 Pixels (Less 2 Pixels)[74]. In a perfect segmentation this index assumes a value of 100% .

The correspondence degree between IMAT and SAT CSAs obtained from automatic and manual segmentations was assessed by performing a Pearson correlation analysis.

Finally, the automatic segmentation results obtained in the entire volume of interest were used to perform a preliminary study of thigh tissue composition. In particular, for each subject the following data were considered: age, BMI, Body Fat percentage, CSA of IMAT, SM and SAT and the ratio between IMAT and SM. The

percentage of Body Fat was assessed through bioelectrical impedance analysis performed with a Handy 3000 DS medica device. The data required by the instrument as input: sex, age, weight and height, were previously assessed for each subject. The body fat percentage was calculated from the impedentiometric data using the Segal equation [75] for NW and the Gray equation [76] for OB subjects. A Kruskal Wallis test and the post hoc Dunn Bonferroni were performed on mean CSAs of IMAT, SM and SAT of the three subject classes in order to investigate significant dissimilarities between group pairs. The statistical significance was set $p < 0.05$.

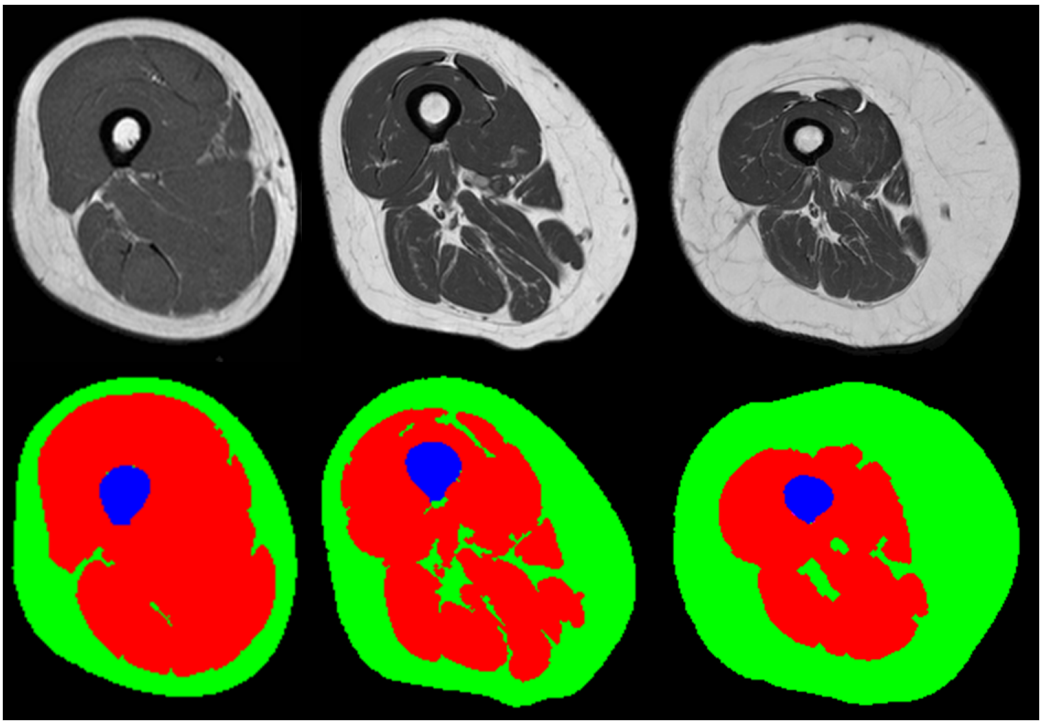

Figure 3.8: Examples of results obtained by automatic classification. On top, from left to right, original T1-W images belonging to a Y-NW, a O-NW and a O-OB subject are shown. On the bottom the correspondent automatic tissue classification are highlighted. Green indicates AT while red and blued indicate SM and bone tissue, respectively.

3.5 Results

Qualitative examples of tissue classification results are shown in Fig.3.8 for the three classes of subjects included in our test set. In Table3.2 the correspondent quantitative

analysis are summarized; the accuracy indexes were calculated for each subject typology as well as for the entire dataset. A mean sensitivity above 96% with a RAD of 2.5%, 1.8% and 2.7% in segmenting bone, SM and AT proved a good correspondence between automatic and manual segmentations. The overall segmentation accuracy was found similar for each class of subjects.

Tissue	Group subjects	sensitivity[%]	Specificity [%]	Accuracy [%]	Precision [%]	RAD [%]
SM	All	96.6 ± 0.2	99.7 ± 0.2	99.2 ± 0.5	98.0 ± 0.8	1.8 ± 1.1
	Y-NW	98.3 ± 0.7	99.9 ± 0.4	99.8 ± 0.0	98.6 ± 0.4	1.0 ± 0.5
	O-NW	95.7 ± 1.0	99.6 ± 0.1	98.8 ± 0.2	98.4 ± 0.5	2.8 ± 0.4
	O-OB	96.0 ± 1.1	99.5 ± 0.1	98.9 ± 0.2	97.0 ± 0.5	1.7 ± 0.5
AT	All	96.0 ± 1.7	99.1 ± 0.7	98.8 ± 0.7	95.3 ± 2.0	2.7 ± 1.9
	Y-NW	94.5 ± 2.0	99.9 ± 0.0	99.7 ± 0.1	96.5 ± 0.6	2.3 ± 1.3
	O-NW	97.1 ± 0.8	98.5 ± 0.5	98.3 ± 0.4	93.8 ± 2.2	3.9 ± 2.6
	O-OB	96.4 ± 0.8	99.0 ± 0.3	98.5 ± 0.2	95.7 ± 1.9	2.0 ± 0.9
BONE	All	96.8 ± 1.1	99.9 ± 0.0	99.9 ± 0.1	98.6 ± 0.8	2.5 ± 1.0
	Y-NW	96.8 ± 1.3	99.9 ± 0.0	99.9 ± 0.1	98.0 ± 0.8	2.5 ± 0.9
	O-NW	96.5 ± 1.2	99.9 ± 0.0	99.1 ± 0.1	99.2 ± 0.3	2.7 ± 1.4
	O-OB	97.0 ± 0.9	99.9 ± 0.0	99.9 ± 0.1	98.8 ± 0.6	2.2 ± 0.9

Table 3.2: Algorithm accuracy result in classifying SM, At and Bone. Data are presented as mean ± standard deviation.

A good correspondence between automatic and manual segmentation was obtained for muscle fascia as it is shown in Fig.3.9, where examples of muscle fascia segmentation in Y-NW, O-NW and O-OB subjects are reported, and in Table3.3 where quantitative results are summarized. Namely, we obtained an overall mean ASD of 0.81mm, lower than pixel resolution and a mean Less 2 Pixels of 86.2%. The algorithm showed slightly lower performance with O-OB subjects where a mean ASD of 1.14 mm was obtained. This result, however, remains in the order of magnitude of pixel resolution.

Fig.3.10 shows the results of correlation analysis performed on CSA of IMAT and SAT compartments assessed from manual and automatic segmentation. In particular, for each group of subjects the scatter plot with the correspondent linear regression are reported. Highly significant Pearson correlation coefficients were found correlating CSA obtained from automatic and manual segmentations in all group of subjects ($p < 0.001$). It is worth to note that SAT correlation is always higher than IMAT

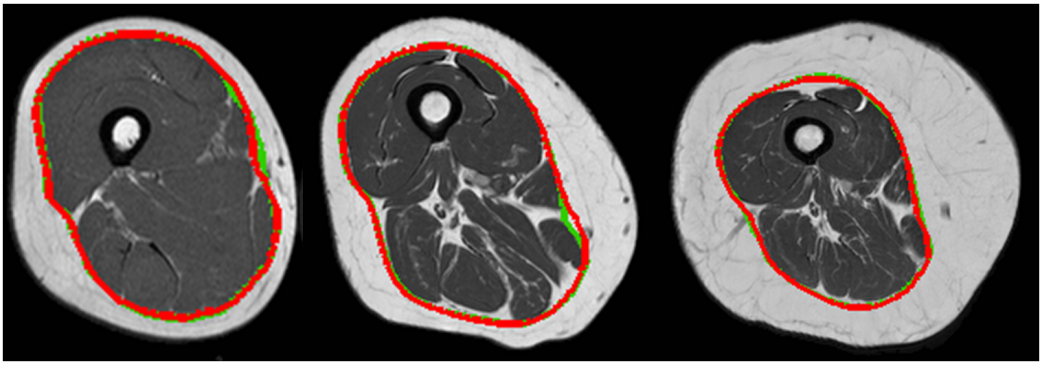

Figure 3.9: Some example of muscle fascia segmentation results in Y-NW (right), O-NW (center) and O-OB(left) subjects.Automatic segmentation indicated in red is superimposed to manual segmentation indicated in green.

Group subject	ASD[mm]	Less 2 Pixels
All	0.81 ± 0.37	82.6 ± 10
Y-NW	0.50 ± 0.06	96.2 ± 2.9
O-NW	0.79 ± 0.20	84.8 ± 5.0
O-OB	1.14 ± 0.41	77.5 ± 9.3

Table 3.3: Results for the proposed method for the segmentation of muscle fascia reported as mean ± standard deviation for each subject typology.

correlation. This can be explained considering that the SAT CSA is one order of magnitude larger than IMAT CSA. Therefore, the same absolute error in the two different compartments corresponds to a very different error measurement expressed in terms of percentage leading to a lower correlation for IMAT.

Table3.4 reports the preliminary results of the thigh composition analysis obtained by quantifying the different compartments of interest from the automatic segmentation results. As expected, in general, IMAT/SM ratio increased with age, BMI, and body adiposity. Indeed, Y-NW subjects presented more SM and less SAT and IMAT than O-NW subjects; O-OB subjects presented more SM and much more IMAT and SAT mass than O-NW, although statistical significance was reached only in the comparison of adipose components (IMAT: p=0.04 for Y-NW vs. O-NW, p=0.001 for Y-NW vs. O-OB, SAT: p=0.01 for Y-NW vs. O-OB).

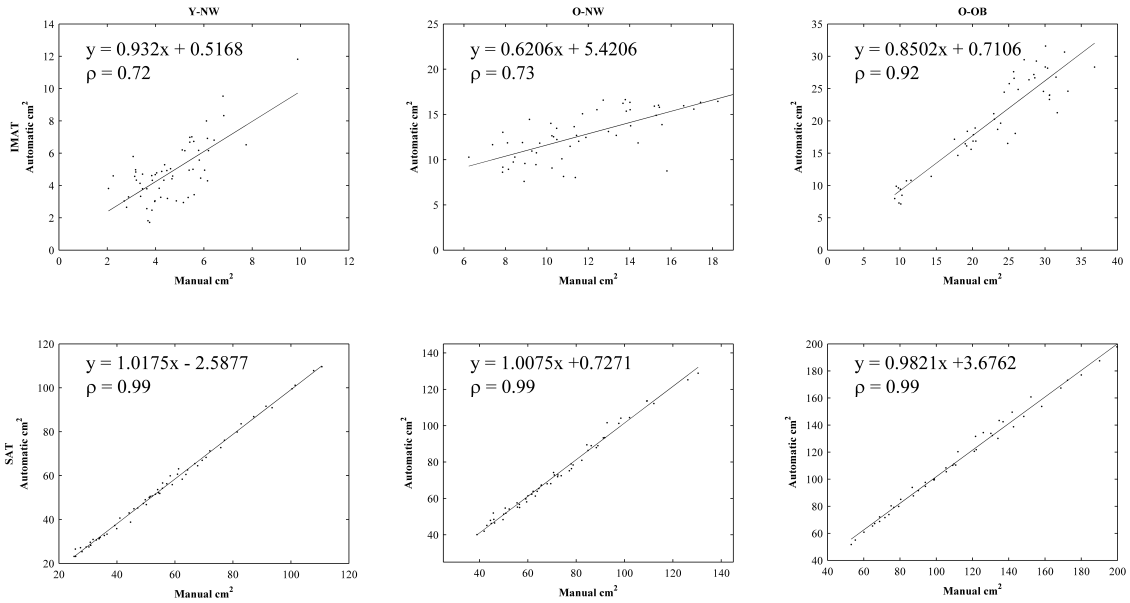

Figure 3.10: Correlation analysis, separately carried out for the three typologies of subjects, on CSA of IMAT and SAT compartments extracted from automatic and manual segmentations.

	AGE	$BMI[kg/m^2]$	Body Fat[%]	IMAT[cm^2]	SM[cm^2]	SAT[cm^2]	IMAT/SM[%]
Y-NW	27 ± 4	19.5 ± 1.0	21.9 ± 4.6	5.0 ± 1.3	99.8 ± 15.1	53.6 ± 21.1	5.1 ± 1.6
O-NW	73 ± 2	24.3 ± 1.8	33.4 ± 1.9	12.8 ± 2.7	87.6 ± 7.7	72.1 ± 11.0	14.5 ± 2.3
O-OB	74 ± 4	36.0 ± 2.0	42.4 ± 3.0	20.6 ± 7.2	99.7 ± 9.7	115.4 ± 35.1	20.4 ± 6.7

Table 3.4: Result of thigh composition analysis. All data are reported as mean $\pm$ standard deviation for each subjet typology

3.6 Discussion

In this chapter we addressed the segmentation of the different tissue compartments of the thigh. A new completely automatic segmentation method, based on fuzzy intensity classification and active snake contour, was proposed to differentiate SM, bone, IMAT, and SAT from T1-W MRI images, in subjects with widely different features in terms of age, BMI, and body adiposity. This method was developed with the aim of providing a reliable tool able to automatically distinguish the different tissue compartments for detecting and monitoring changes in regional composition caused by aging and metabolic abnormalities.

Many works in previous literature have been proposed with the aim to distinguish

SM and AT from MRI images of the lower limb. All of them exploited the very large intensity contrast between these two tissues of interest by proposing different methodologies based on low level information [61, 62, 63, 64]. In particular, Urricelqui et al [63] proposed a multilevel classification approach based on shaped histograms and adaptive thresholding to distinguish SM from AT. They validated the algorithm on a dataset composed of young OB women using manual segmentation as reference and obtained a mean precision of 90%. Brunner et al [61] concentrated their work on the segmentation of SM proposing a probabilistic classification approach where prior probabilities are based on voxel-derived texture features. They validated the algorithm on images acquired in patients affected by peripheral arterial disease using a semi-automatic segmentation as reference and obtained accuracy, sensitivity, and specificity of 88.32%, 93.31%, and 87.29%, respectively. SM segmentation was also faced by Makrogiannis et al [65] proposing an approach based on intensity centroid clustering and morphological operators. They validated the algorithm on male and female middle-age subjects comparing the automatically obtained SM area at the mid-thigh with a semi-manual segmentation performed on a correspondent CT image. They reported a mean ASD equal to 4.39%. Comparing these results with the accuracy of the segmentation method proposed in this work on SM, it seems our approach reached comparable or better performance for each group of subjects. Indeed, we reported an average ASD between the areas extracted from reference and automatic segmentation of 1.8% and an accuracy, sensitivity, specificity, and precision of 96.63%, 99.7%, 99.2%, and 98.0%, respectively.

A comparison, regarding bone segmentation results, between the proposed approach and previous literature cannot be carry out as no data has been reported in this sense. However, our approach proved to be accurate and reliable. Indeed, we obtained an average sensitivity of 96.8% with an accuracy, specificity, and precision above 99% without encountering bone segmentation failures as contrarily reported by previously presented approaches [67, 66]. A failure of bone segmentation, which in most cases is due to very thin cortical region that assumes an intensity range typical of SM, leads to an important overestimation of IMAT compartment and a less significant overestimation of SM.

Despite the relevant significance of IMAT quantification in the study of processes related to aging and obesity, the automatic discrimination of IMAT and SAT is still a challenging task. Indeed, only few works faced the problem [65, 66, 67], and all of them identified the muscle fascia, which separates IMAT from SAT, using a geometrical definition. Namely, they assumed the muscle fascia as a structure which smoothly envelops SM with a perfect adherence in the external SM parts, resulting in an underestimation of IMAT in all those subjects where a condition of high degree of fat infiltration is present. Following this assumption, [66] proposed an approach based on morphological operators with a fixed scale structuring element, while [65, 67]

used approaches based on active contour models: the balloon deformable model and the gradient vector flow respectively. They reported qualitative good performance of their methods but they lacked in performing exhaustive analysis on quantitative segmentation accuracy. However, a direct comparison of segmentation accuracy between our approach and previous works would still be cumbersome, especially regarding conceptual differences, discussed above, on the definition of muscle fascia. We believe that our approach, based on the detection of muscle fascia in its anatomical position, results more robust with respect the variability of subject features, and nevertheless more accurate in presence of high degree of fat infiltration. In fact, thanks to the preprocessing step, aimed at rising the contrast between muscle fascia and AT and at the same time reducing the contrast between SM and AT, the snake evolution is driven toward the weak edge of muscle fascia both when it adhere to SM and when it is separated from SM by a layer of AT.

Despite the good accuracy reached by our algorithm, certain limitations should be recognized.

Due to the high difficulty found in recruiting appropriate volunteers, the high costs of MRI examinations and the huge demands on time required for manual segmentations, we performed the parameter setting procedure qualitatively and using three datasets. A quantitative parameter setting procedure, including the comparison between manual and automatic results, will allow to further improve and demonstrate the accuracy of our algorithm. For the same reasons, we validated our algorithm in a dataset with limited size (15 studies). Even if the dataset was composed of subjects with a wide variety in terms of age, body composition and fat infiltration degree, a confirmation of our result in an extended dataset should be performed. An extended manual segmented dataset would also allow to perform a cross validation study, avoiding problems of asymmetric samples typical of datasets split in only two parts. In addition, it would be of interest to validate our algorithm in subjects affected by neuromuscular disorders, as this kind of tools are strongly demanded also in such contexts.

The use of a classical T1-W spin echo protocol instead of a sequence, which provides a clear separation between fat and water signal, could be seen as a limitation. However, T1-W protocols are present on every MRI machinery and are the preferred technique in studies of regional composition, and therefore our methods could have a major relevance in clinical practice as well as in retrospective studies. It is also worth to note that the contrast between AT and muscle fascia is similar in both T1-W spin echo and in fat images acquired with chemical shift encoded protocols; therefore we could speculate that our algorithm could be easily adapted and applied to IP images obtaining similar performances.

An aspect that should be improved is the performance of the algorithm in terms of run-time as it was not optimized in the present study. However, our method

is not operator time consuming, as it is totally automatic, making this aspect not critical. At the same time, it would be of interest to quantify the time saved from the operator by using our automatic approach, by comparing the time spent by the operator for delineate all the contour of interest with the run-time of our algorithm which is equal to 60 sec per slice. It is also worth to note that our algorithm was validated by using as reference segmentations the manual contours delineated by a single operator. This is the consequence of the fact that, the manual segmentation process is very time-consuming and the involvement of more imaging experts was for us impossible. Being the manual segmentation an operator dependent process, it would be interesting to investigate the intra and inter operator variability in order to prove the interchangeability between our automatic approach and an expert operator.

Finally, it should be considered that our algorithm is likely to fail on datasets coming from subjects with metallic orthopedic devices or implants, which by interfering with the MRI magnetic field induce a large signal distortion causing saturation regions (bright and dark areas) on the image in the neighborhood of the magnetic material. However, MRI protocols in this king of subjects are usually avoided.

Our preliminary results obtained in terms of quantitative characterization of thigh regional tissue composition provide an example of the effectiveness of the method for practical use; it is possible to appreciate a decrease of SM for effect of age-related sarcopenic processes (Y-NW vs. O-NW) and, at the same age, an opposite effect of obesity (O-NW vs. O-OB), in line with previous reports based on a definitely more complex and time-consuming image analysis [29]. Consistent variations can be appreciated also for AT, with an overall increase due to the effect of both age and obesity. Moreover, the capability of the method to perform an adequate IMAT analysis is of particular interest, due to the predictive value of this AT component for metabolic degeneration associated with overweight and obesity [7, 8, 9].

In conclusion, our findings evidence the accuracy of the proposed method and the effectiveness of its application on real MRI data. The use of this approach to automatically extract tissue components allowing the assessment of thigh regional composition from T1-W MRI data makes possible a reduction of the contouring time with respect to manual delineation while permitting an accurate definition of IMAT and SM compartments.

Chapter 4

Effects of muscle composition and architecture on specific strength in obese older women

The morphological characterization of the different tissue compartments and their correspondent quantification is not sufficient to fully explain the dynamics of processes related to aging and obesity which cause a reduction of muscle functionality. Therefore, in muscle performance analysis, functional features, such as architectural parameter and muscle composition, must be considered. In this chapter an analysis on structural and architectural muscle parameters will be performed in OB and NW older females in order to investigate the effect of obesity on strength production in older women [2].

4.1 Introduction

The effect of obesity on physical functioning in older people is poorly understood. It has been shown that OB adults have more muscle mass and higher muscle strength than NW adults [12]. However, the strength normalized with respect to body mass is lower in OB than in non OB individuals indicating that muscles in OB subjects suffer from functional deficit. Some of factors that are found to be correlated with muscle functional deficit are muscle architecture and composition. Indeed, muscle architecture is recognized as an important factor in concentric strength deficit in older individuals [77, 78]. Namely, the relationship between strength and velocity of SM depends on sarcomeres both in parallel, represented by CSA, and in series, represented by muscle FL [48]. It has also been shown that FL is shorter in older compared with young adults [79, 80].

In addition, it is known that the increase in muscle size affects muscle architecture by increasing the fascicle PA in both young and older individuals [81, 82, 83, 84].

A correlation between muscle composition and strength production in older adults was found by [30]. They found that lower muscle attenuation, measured at mid-thigh by computed tomographic scanning and indicating greater fat infiltration in muscle tissue, was negatively correlated with isokinetic muscle strength.

The aim of this study was to investigate if changes on muscle architecture and composition in older OB women can result in a lower strength production despite increased muscle mass.

4.2 Subjects

The present study included eleven healthy female elderly volunteers, six NW and five OB. After a fully explanation regarding the nature of the protocol, each of them signed the informed consent form approved by the Institutional Review Board of Istituto Auxologico Italiano. Volunteers with declared myopathic, cardiovascular, inflammatory and neurological condition were excluded.

For each participant, height and weight were measured and the total body fat percentage was assessed with dual-energy X-ray absorptiometry. In addition, the International Physical Activity Questionnaire (IPAQ) was filled by all participants in order to evaluate their daily physical activity level. Table4.1 summarized the participants characteristics within the groups.

Group	n	Age[years]	Weight[kg]	Height[cm]	BMI[kg/m^2]	Body fat[%]	IPAQ [SCORE]
OB	5	72.4 ± 2.3	82.9 ± 4.9	150.2 ± 4.0	36.8 ± 1.9	41.9 ± 2.9	1659 ± 1331
NW	6	72.7 ± 1.9	$60.3 \pm 4.8^*$	$155.4 \pm 3.0^*$	$24.3 \pm 1.8^*$	$33.4 \pm 1.9^*$	1655 ± 647

Table 4.1: Characteristics of the subjects involved in the present study. Data are presented as mean ± standard deviation. * indicates statistically significant difference from OB with $p < 0.05$.

4.3 Experiments

4.3.1 Muscle dimension and fat content

For each participant, size and percentage of fat content of the muscle QF were assessed at the mid-thigh of dominant leg from Dixon MRI images. Subjects underwent thigh MRI investigation on an MR Philips Achieva scanner. They were positioned supine

with their knee fully extended in the magnet. A coronal scout image was initially acquired in order to identify the mid-thigh position located on the middle of femur length. This length corresponds to the distance from the bottom of the lateral femoral condyle and the most proximal edge of the greater trochanter. A three-point Dixon sequence [41] was used to image the section correspondent to mid tight. The MRI scanner, after performing an elaboration of the three acquired images, provided the resulting images of water and fat. Fat and water images were loaded into MIPAV program, and quantitative fat percent images were computed as following:

$$fatpercentage = fatimage/(fatimage + waterimage)$$

In these images, an expert operator manually delineated the QF contour. The area of the correspondent region was the QF CSA and the average of the pixels intensity values represented the Percentage of fat content of quadriceps femoris (MF).

Group	$CSA[cm^2]$	MF[%]
OB	45.8 ± 4.6	10.8 ± 1.9
NW	$39.1 \pm 2.4^*$	$8.4 \pm 1.6^*$

Table 4.2: Dimension of the QF expressed in terms of CSA and the correspondent percentage of fat content MF. Data are presented as mean ± standard deviation. * indicates statistically significant difference from OB with $p < 0.05$.

4.3.2 Muscle Architecture

The muscle architectural parameters considered in this study were PA and FL and were assessed using two-dimensional B-mode ultrasonography (MyLabFive, Esaote, Italy). During the acquisition protocol the subjects were positioned supine with their knee fully extended. Firstly, the proximal and distal edges of Rectus Femoris (RF), Vastus Intermedius (VI), Vastus Medialis (VM) and Vastus Lateralis (VL), which are the four muscle bellies composing QF, were identified by the operator by moving the probe along the thigh. These reference points were marked on the subject skin. Then, the length of each muscle belly was measured, divided into three portions (proximal,middle and distal) and marked on the skin. For each muscle site, the operator moved the probe to obtain a correct alignment with muscle fascicles. Appropriate probe alignment was achieved when several fascicles could be traced without interruption across the image. US images were obtained from each site for each muscle belly.

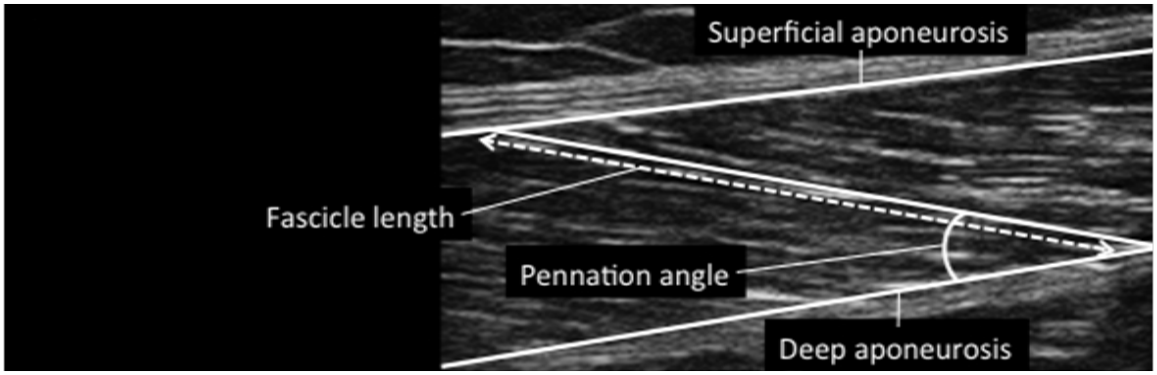

(a)

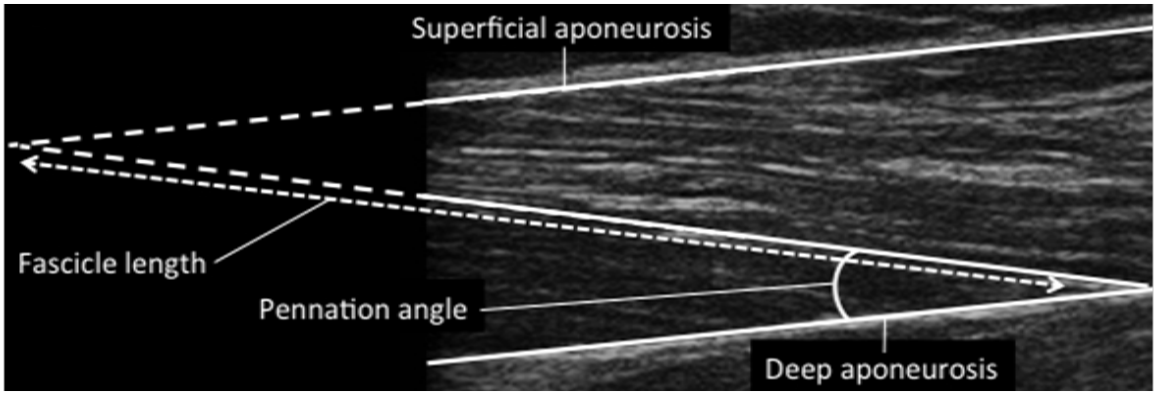

(b)

Figure 4.1: Two examples of PA and FL measurement from US images of two different muscles. a) The entire length of the fascicle is visible in the image. b) The fascicle is partially visible in the image and the interpolation procedure is shown.

MIPAV software was used to measure the muscle architectural parameters from images. PA was measured as the angle between the muscle fascicular paths and their insertion into the deep aponeurosis (fibrous structure, expanded tendon, giving attachment to muscle fibres), which is representative of the muscle's axis of force generation (Fig.4.1). When the field of view of the image included the entire fascicle, the FL was directly measured (Fig.4.1a). On the other hand, when the fascicle extended off the field of view the FL was determined through a linear interpolation of fibres and aponeurosis [85] (Fig.4.1b). The entire procedure was carried out in four fascicles in a single image and the mean value of the extracted parameters was considered representative for the image. The relative contribution of each muscle belly to the total QF volume was obtained from the literature [86]. For each parameter, a weighted mean for the relative volume of each muscle belly was calculated and

considered representative of the entire QF.

Parameter	Group	RF	VL	VI	VM	QF
PA[deg]	OB	15.9 ± 2.7	12.5 ± 1.3	9.0 ± 2.4	13.8 ± 1.8	12.3 ± 0.8
	NW	$12.1 \pm 1.5^*$	10.6 ± 2.0	8.0 ± 0.9	$9.5 \pm 2.6^*$	$9.8 \pm 1.4^*$
FL[mm]	OB	53.3 ± 7.5	80.1 ± 12.7	65.6 ± 13.8	73.3 ± 15.2	70.6 ± 13.8
	NW	56.1 ± 10.3	70.2 ± 15.4	65.0 ± 6.1	86.7 ± 15.3	70.7 ± 13.2

Table 4.3: Architectural parameters PA and FL assessed for the entire QF and measured in the four muscle bellies composing QF: RF, VL, VI, VM. Data are presented as mean ± standard deviation. * indicates statistically significant difference from OB with $p < 0.05$.

4.3.3 Muscle isometric and isokinetic torque

After muscle characterization, muscle strength was assessed in terms of peak KET using a Cybex dynamometer (Cybex International, Medway, MA, USA) on the dominant leg of each subject. Participants were seated comfortably in the dynamometer chair, so that a 90 deg angle at the knee joint was obtained. The rotational axis of the dynamometer was aligned with the lateral femoral epicondyle of the subject's knee, with the resistance pad positioned proximally to the lateral malleolus of the ankle joint. The trunk of the subject was erect and fastened by a belt. A second belt was placed around the thigh, to prevent any accessory movement during knee extension.

Before starting the test, the torque passively generated by the gravitational pull of the lower leg was recorded with the knee fully extended. The KET recorded during the test was corrected to the gravitational load.

Following a familiarization session, each subject performed one isometric knee-extension test at 90 deg of knee flexion, and four isokinetic tests at 240, 180, 120 and 60 $degs^{-1}$. For each of them, three attempts were made, but only the highest peak KET was selected for further statistical analysis. Between attempts, 1 min of recovery was observed.

Starting from KET, a measure of specific capability of muscle strength production was obtained by accounting for the ratio of torque to muscle dimensions (specific torque, KET/CSA).

The correlations betweenKET/CSA and compositional and architectural parameters were investigated separately for isometric (KET_0/CSA) and isokinetic tests. In order to have a single value representative of all investigated dynamic conditions, for each subject the specific torque–velocity data were fitted by the equation [3]:

$$k = (KET/CSA + a) \times (v + b)$$

where k, a and b are constants and v is the angular velocity. By extrapolating the function back to zero velocity, a single value representative of dynamic conditions (KET_{DYN}/CSA) was obtained.

	Knee-extension torque[Nm]				
Group	$240degs^{-1}$	$180degs^{-1}$	$120degs^{-1}$	$60degs^{-1}$	$Isometric$
OB	35.9 ± 11.3	44.6 ± 16.1	64.5 ± 18.4	85.1 ± 22.6	106.5 ± 15.3
NW	50.7 ± 13.8	64.5 ± 16.3	80.4 ± 17.7	102.5 ± 14.4	115.7 ± 13.0

Table 4.4: Absolute KET values during isokinetic and isometric test. Data are presented as mean ± standard deviation. No statistically significant differences were found between the two groups.

4.3.4 Parameters Overview

For the sake of clarity, an overview of the parameters measured in this study is reported on Table4.5.

4.3.5 Statistical analysis

Data of OB and NW subjects were compared using a Mann-Whitney test with statistical significance set to $p < 0.05$. Correlation between parameters were investigated by means of linear regression analysis.

4.4 Results

Table4.1 reported the anthropometric differences between OB and NW subjects. The two groups have the same level of habitual physical activity, having no significant differences on IPAQ score. The OB are slightly shorter than NW and as expected are heavier with a greater amount of body fat.

The obtained average results regarding QF size and composition in the two groups are reported on Table4.2. The MRI image analysis showed that, OB had a QF CSA size 17% bigger than their NW counterpart ($p < 0.05$) with a higher MF (28.7%$p < 0.05$).

Parameter	Description
CSA[cm^2]	It is the mid thigh cross sectional area of the quadriceps femoris. It is an indicator of the quadriceps femoris dimension.
MF[%]	It is the percentage of fat tissue measured on the mid thigh cross sectional area of the quadriceps femoris. It is an indicator of muscle composition.
PA[deg]	Pennation angle is a muscle architectural parameter. It is the angle of the muscle fibers within the muscle with respect to the angle of pull. It has been estimated for the quadriceps femoris, starting from the measured four muscle belly PA.
FL[mm]	Fascicle length is a muscle architectural parameter. It is the muscle fiber length. It has been estimated for the quadriceps femoris, starting from the measured four muscle belly FL.
KET[Nm]	Knee-extensor torque. Is is an indicator of the force developed by the quadriceps femoris. It has been measured both in isometric (KET_0) and isokinetic conditions at different angular velocities.
KET_0/CSA	Knee-extensor torque in isometric condition normalized to quadriceps femoris CSA. It is an indicator of the normalized force developed by the quadriceps femoris.
KET_{DYN}/CSA	Knee-extensor torque in isokinetic condition normalized to quadriceps femoris CSA. This single parameter representative of the normalized force developed by the quadriceps femoris in dynamic conditions was estimated with the Hill equation [3].

Table 4.5: Overview of the parameters measured in this study

Table4.3 summarizes the architectural data obtained for the single muscles and for the QF overall. No statistically significant difference was found between the FL of OB and NW. On the other hand, the PA of OB in the whole QF was 24.9% bigger than those of NW ($p < 0.05$).

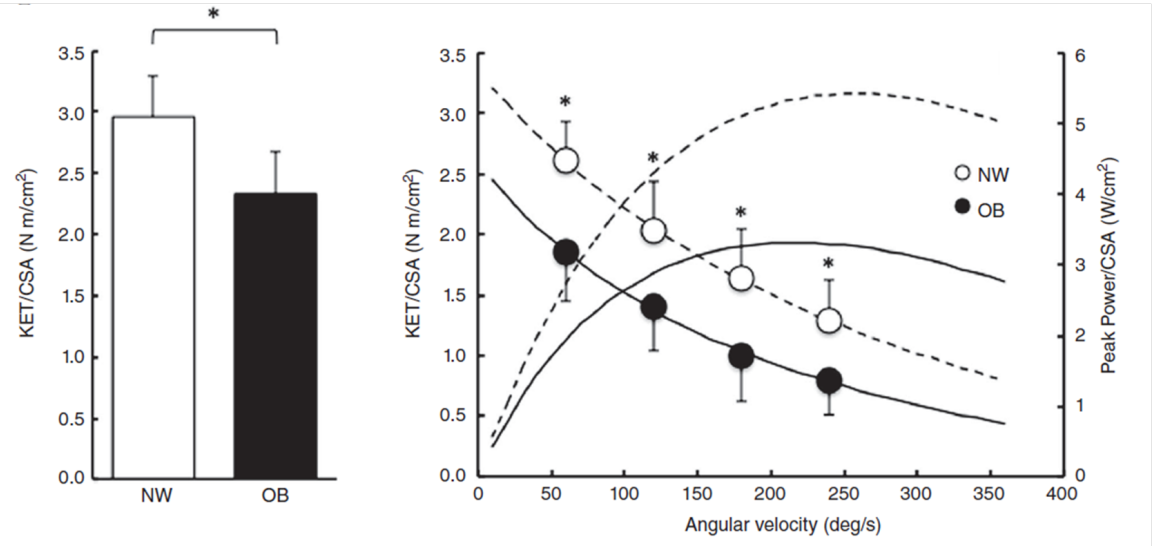

Figure 4.2: The results of the analysis of isometric and isokinetic specific muscle knee-extension torque (KET/CSA) Left: The graph shows muscle quality expressed as isometric specific muscle knee-extension torque (KET/CSA) in NW (white column) and OB subjects (black column). Right: the graph shows KET/CSA as a function of knee-extension angular velocity in NW (white circles) and OB subjects (black circles). Hill equation [3] was used to fit the experimental values: continuous line indicates OB subjects; dashed line indicates NW women. Peak power/CSA was calculated as $KET/CSA \times (angularvelocity/57.3)$. * indicates statistically significant difference from OB with $p < 0.05$.

Table4.4 shows the results of the KET analysis. No statistically significant differences were found between the absolute strength developed by NW and OB subjects, despite the bigger amount of SM found in OB. Consequently the KET normalized on CSA (Specific torque) resulted higher for NW in all test performed (Fig.4.2).

The correlation analysis between both specific isometric and dynamic torque and muscle architectural parameters are reported in Table4.6 while correlation between both specific isometric and dynamic torque and muscle fat content are summarized in Fig.4.3. A good significant inverse correlation was found between KET_0/CSA and both MF ($p < 0.05$) and PA ($p < 0.05$), but not with FL. On the other hand,the KET_{DYN}/CSA was found inversely and significantly ($p < 0.01$) correlated with MF, but no significant correlations with architectural parameters were detected.

Parameter	FL	PA
KET_0/CSA	-0.034	-0.608^*
KET_{DYN}/CSA	-0.335	-0.362

Table 4.6: Pearson correlation coefficient between specific muscle isometric and isokinetic KET and architectural parameters of QF muscle.

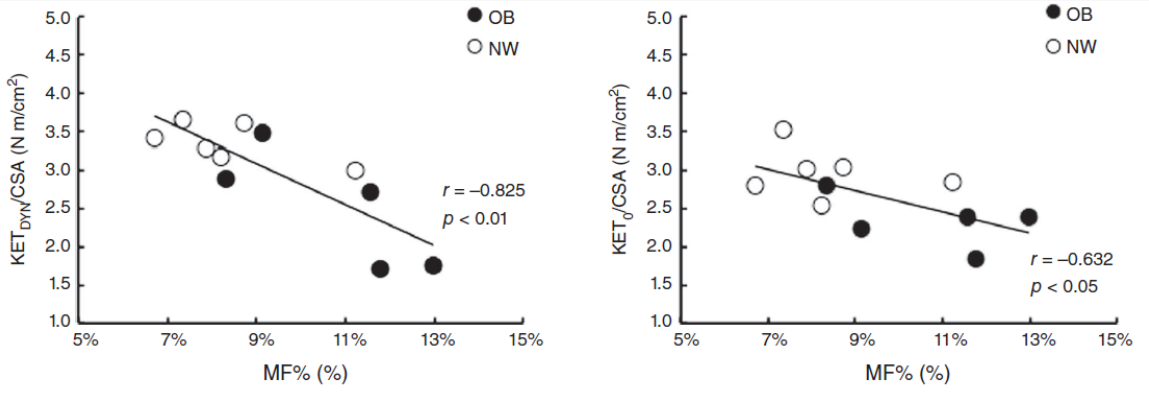

Figure 4.3: Correlation analysis of KET/CSA and quadriceps femoris MF. a) The graph shows the scatter plot and the correspondent linear regression of MF and torque values normalized to CSA extrapolated back to zero velocity starting from isokinetic torque values using the Hill equation [3]. b) The graph shows the scatter plot and the correspondent linear regression of MF and KET/CSA recorded during the isometric test.

4.5 Discussion

In this work, the effects of obesity on skeletal muscle architecture and composition in older women were evaluated.

In agreement with previous works [87, 12, 29], we found that OB have more muscle mass than NW subjects. The larger muscle mass in OB can be explained by considering the larger body mass as a constant stimulus for muscles which induces the muscle grown and consequently the development of larger absolute strength. However, due to the concomitant increase in AT, the fraction of SM reduces as well as the strength normalized to body weight [87, 12, 88].

In this study, we found comparable values of KET in OB and NW subjects which resulted in a larger KET/CSA in NW as already reported in [87, 89]. This difference indicates that strength production is influenced by not only muscle size but also by other factors. Fat infiltration has been found to be one of such a factors [30]. In this

study, the MF quantification obtained through Dixon MRI images analysis revealed a significantly greater amount of fat in OB than NW subjects. Moreover, a significant negative linear correlation was detected between MF and KET/CSA in both isokinetic and isometric conditions.

In our data, PA, measured by means of US appeared to be significantly greater in OB than in NW subjects. The same result was obtained by [84]. It is also been shown that an increase in muscle size induces an increase in PA [81, 79, 90]. In pennate muscles, as it is QF, the fascicles move obliquely to the axis of shortening of the muscle belly during contraction; therefore, the force they develop is used only partially for muscle shortening [91]. In subjects specifically trained for muscle hypertrophy, force relative to muscle CSA was negatively related with PA [90], although a concomitant increase in CSA occurring in these conditions [81] has an opposite effect on overall muscle strength, and the net balance between these factors can hardly be described with simple linear models [91]. Accordingly with these evidences, an increased PA can be considered as a possible determinant of the lower KET/CSA observed in OB subjects and our study supports this theory. In fact, during isometric test, the negative effect of PA on KET_0/CSA was confirmed, while during isokinetic contractions no significant effect of PA on KET_{DYN}/CSA was clearly detected. It is possible that the negative effect of steeper PA on muscle strength generation may be less detectable in isokinetic conditions, when the disadvantage of a large PA in the transmission of force is counterbalanced by the advantage for muscle shortening velocity [92]. However, these results need to be confirmed in a more numerous cohort of subjects.

It has been shown that FL decreases with age [48] causing a deficit in strength development [78]. However, we did not found significantly differences in terms of FL between our groups indicating that obesity in older women does not induce additional effects on FL and then FL seems not to be involved in the reduction of specific strength observed in OB compared with NW older women.

In conclusion, we can state that muscle composition and architecture seem to be important factors on the development of strength in elderly women. Due to the effect of obesity overload, OB women have a larger muscle size than NW women, but disadvantageous muscle composition and architecture. The higher MF and steeper PA observed in OB women are associated with reduced levels of muscle specific strength.

Chapter 5

Conclusions

This thesis was aimed at the development and application of segmentation and automatic analysis methods for the morphological and functional characterization of the lower limb from MRI images in physiological field, and in particular for the study of processes related to aging concomitant to obesity condition.

The continuous development of imaging technique, and in particular the extraordinary progresses made in MRI field has allowed to make giant steps on the study of muscular physiologic processes. In fact, with the many MRI techniques today available which allow to obtain many contrasts it is possible to investigate SM morphological and functional aspects as well as to map these aspects in 3D in entire body regions.

This enormous amount of data has lead to the need of tools aimed at automatically extracting information of interest from the images. As an example, the morphological characterization of the tissues of interest, which is the first step in the study of physiological processes related to aging and obesity leading to low muscle functionality and so disability, is performed through a segmentation process aimed at discriminating and quantifying the different tissues of interest. This process, if manually executed is extremely time consuming and results unfeasible in ordinary clinical contexts.

In Chapter 3 we presented a segmentation algorithm aimed at automatically segmenting the thigh tissues from T1-W MRI images in both young and elderly subjects with different characteristics in terms of body adiposity, including OB subjects. In particular, the algorithm was able to classify bone, SM and AT. In addition, the 2 compartments of AT: IMAT and SAT were discriminated by identifying the muscle fascia. The segmentation approach is based on fuzzy c mean algorithm for tissue classification and on active snake evolution for the identification of the muscle fascia. Thanks to a smart process aimed at reducing the contrast between AT and SM and simultaneously obtaining an enhancement of the relative contrast between muscle fascia and AT we drove the active contour to converge in the weak edge of muscle

fascia. To our knowledge, this is the first published approach which identifies muscle fascia in its anatomical position obtaining promising results from a low level based segmentation perspective.

The quantitative evaluation of the segmentation method was performed using different similarity metrics adopted in previous works, and its superiority against the other state-of-art methods demonstrated. However, it is worth to note that a fair comparison, especially on IMAT and SAT segmentations, is not possible because of the different assumptions made on reference segmentations. Due to the high accuracy shown in our results, we are confident that our method could offer reliable performance in the field of thigh regional composition.

As a second research line dedicated to the muscle functional characterization, we presented in Chapter 4 a study aimed at investigating the effects of obesity on the muscle strength developed by elderly women. Namely, functional and structural features of the QF were evaluated against peak KET measured in isometric and isokinetic condition in NW and OB women with the same degree of physical activity. In particular, for each subjects, QF muscle size and percentage of fat content were measured by analyzing Dixon MRI images while architectural parameters PA and FL were assessed by processing US images.

The analysis showed that muscle tissue composition and PA strongly influence the specific muscle torque in healthy elderly women. Namely, a steeper PA and a higher fat infiltration in the muscle are negatively correlated with both isometric and isokinetic contractions.

OB presented a larger muscle mass than NW subjects, due to the greater constant body mass load. Moreover, OB subjects demonstrated a bigger PA with a larger fat content in the QF leading to a reduction of the developed specific strength.

Nowadays, health among the elderly is of absolute relevance for the health care systems all over the word, since life expectancy among the elderly has been improving for many decades and medical costs grown with age. Therefore, the early detection and an accurate follow up of morphological and functional changes in the musculoskeletal system correlated to disorders and pathological conditions is fundamental. We believe that in this context our research could have an important clinical impact.

Firstly, our automatic algorithm, able to accurately segment the thigh tissues and in particular to distinguish IMAT from SAT could be potentially introduced in clinical practice to quantify SM, IMAT and SAT in protocols aimed at understanding and monitoring processes related to age and overweight. The fact that the algorithm is totally automatic allows clinicians to have a specific tissues quantification for a large cohort of patients, potentially leading to the design of patient specific intervention and monitoring programs.

As a second contribution in clinical application, the identification of changes on muscular parameters due to obesity and correlated with poor muscular functioning

and disability could be of interest in the design of specific protocols aimed at rehabilitating muscle physiology. Moreover these parameters can provide important information for interpretation of results from interventional investigations.

Finally, we can conclude that this work represents a step forward not only to the accomplishment of accurate patient-specific segmentation of the thigh, but also to the understanding of processes related to aging with the concomitant presence of obesity.

5.1 Future Work

The first improvement of this work should be a confirmation of our results in a larger sample of subjects. Then, the algorithm could be extended to the calf by adapting the bone segmentation procedure and resetting the parameters properly. Important future development could be also the comparison between different state of art segmentation algorithms in order to design the extension of our segmentation algorithm in 3D. In addition, starting from the SM segmentation, the different muscles could be distinguished, in order to study the distribution of atrophy and determine if this condition affects preferential regions. Atlas based methods could be a valid candidate for this task.

With respect to functional muscle characterization, it would be of interest to study the relationship between muscle composition and the correspondent activation. A protocol involving Dixon technique and mfMRI could give important information regarding this physiological question.

Appendix A

Muscle Architecture

Muscle architecture is defined as the organization of the muscle fibers within the muscle relative to the line of force generation [48] and it has been recognized as one of major factors determining muscle functional performance. Therefore, the understanding of this structure–function relationship has a relevant clinical importance. In fact, it clarifies the physiological basis of force production and movement, provides a scientific rationale for surgery that may involve tendon-transfer procedures, provides guidelines for electrode placement during electromyographic measures of muscle activity, explains the mechanical basis of muscle injury during normal movement, and aids in the interpretation of histological specimens obtained from muscle biopsies. In Fig.A.1 the structural organization of the muscle tissue is shown. The muscle belly contains the sum of all the muscle fibers; large muscles such as quadriceps are composed of different muscle bellies. The muscle fibers are grouped into bundles of around 150 fibers called fascicles. In pennate muscles, fascicles are attached obliquely to their tendon and the parameters related to this disposition are correlated with muscle functionality. This parameters are mainly FL, PA, and PCSA. The PA is defined as the angle between the fascicle and the force-generating axis parallel with tendon (See Fig.A.2), and the PCSA is the sum of the traverse areas of single muscle fibers measured perpendicular with respect to their longitudinal direction.

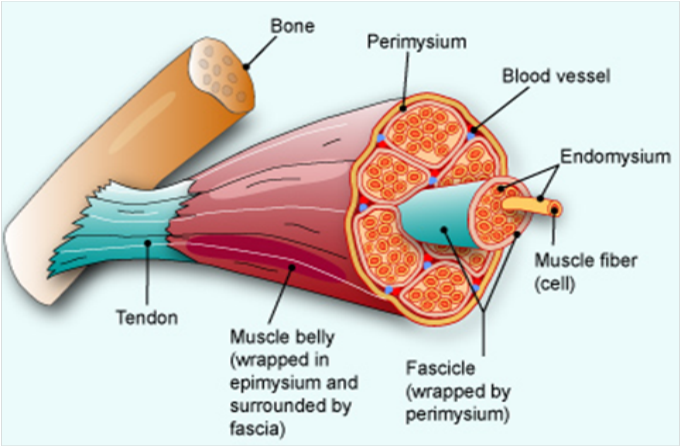

Figure A.1: The structural organization of the muscle

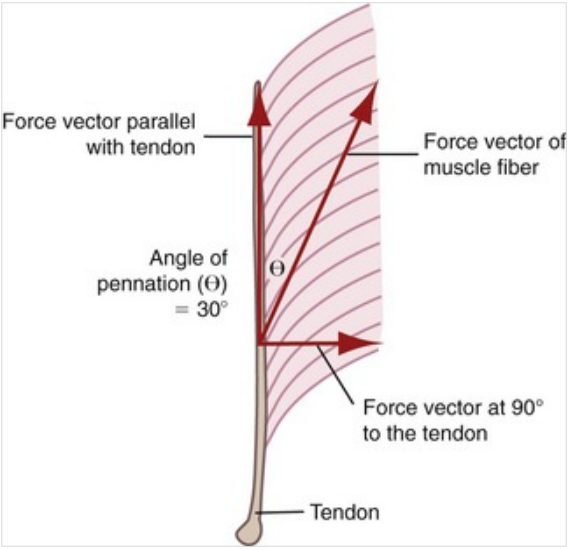

Figure A.2: Pennation angle

Bibliography

[1] S. Orgiu, C. L. Lafortuna, F. Rastelli, M. Cadioli, A. Falini, and G. Rizzo, "Automatic muscle and fat segmentation in the thigh from t1-weighted mri," *Journal of Magnetic Resonance Imaging*, 2015.

[2] F. Rastelli, P. Capodaglio, S. Orgiu, C. Santovito, M. Caramenti, M. Cadioli, A. Falini, G. Rizzo, and C. Lafortuna, "Effects of muscle composition and architecture on specific strength in obese older women," *Experimental physiology*, vol. 100, no. 10, pp. 1159–1167, 2015.

[3] A. Hill, "The heat of shortening and the dynamic constants of muscle," *Proceedings of the Royal Society of London B: Biological Sciences*, vol. 126, no. 843, pp. 136–195, 1938.

[4] E. Mercuri, A. Pichiecchio, J. Allsop, S. Messina, M. Pane, and F. Muntoni, "Muscle mri in inherited neuromuscular disorders: past, present, and future," *Journal of Magnetic Resonance Imaging*, vol. 25, no. 2, pp. 433–440, 2007.

[5] M. Elliott, G. Walter, H. Gulish, A. Sadi, D. Lawson, W. Jaffe, E. Insko, J. Leigh, and K. Vandenborne, "Volumetric measurement of human calf muscle from magnetic resonance imaging," *Magnetic Resonance Materials in Physics, Biology and Medicine*, vol. 5, no. 2, pp. 93–98, 1997.

[6] G. Rådegran, E. Blomstrand, and B. Saltin, "Peak muscle perfusion and oxygen uptake in humans: importance of precise estimates of muscle mass," *Journal of applied physiology*, vol. 87, no. 6, pp. 2375–2380, 1999.

[7] M. Boettcher, J. Machann, N. Stefan, C. Thamer, H.-U. Häring, C. D. Claussen, A. Fritsche, and F. Schick, "Intermuscular adipose tissue (imat): association with other adipose tissue compartments and insulin sensitivity," *Journal of Magnetic Resonance Imaging*, vol. 29, no. 6, pp. 1340–1345, 2009.

[8] B. H. Goodpaster, F. L. Thaete, and D. E. Kelley, "Thigh adipose tissue distribution is associated with insulin resistance in obesity and in type 2 diabetes

mellitus," *The American journal of clinical nutrition*, vol. 71, no. 4, pp. 885–892, 2000.

[9] J.-E. Yim, S. Heshka, J. B. Albu, S. Heymsfield, and D. Gallagher, "Femoral-gluteal subcutaneous and intermuscular adipose tissues have independent and opposing relationships with cvd risk," *Journal of Applied Physiology*, vol. 104, no. 3, pp. 700–707, 2008.

[10] R. L. Marcus, O. Addison, L. E. Dibble, K. B. Foreman, G. Morrell, and P. LaStayo, "Intramuscular adipose tissue, sarcopenia, and mobility function in older individuals," *Journal of aging research*, vol. 2012, 2012.

[11] S. Stenholm, T. B. Harris, T. Rantanen, M. Visser, S. B. Kritchevsky, and L. Ferrucci, "Sarcopenic obesity-definition, etiology and consequences," *Current opinion in clinical nutrition and metabolic care*, vol. 11, no. 6, p. 693, 2008.

[12] C. Lafortuna, N. Maffiuletti, F. Agosti, and A. Sartorio, "Gender variations of body composition, muscle strength and power output in morbid obesity," *International journal of obesity*, vol. 29, no. 7, pp. 833–841, 2005.

[13] N. Mitsiopoulos, R. Baumgartner, S. Heymsfield, W. Lyons, D. Gallagher, and R. Ross, "Cadaver validation of skeletal muscle measurement by magnetic resonance imaging and computerized tomography," *Journal of applied physiology*, vol. 85, no. 1, pp. 115–122, 1998.

[14] R. Ross, B. Goodpaster, D. Kelley, and F. Boada, "Magnetic resonance imaging in human body composition research: from quantitative to qualitative tissue measurement," *Annals of the New York Academy of Sciences*, vol. 904, no. 1, pp. 12–17, 2000.

[15] I. Janssen, S. B. Heymsfield, Z. Wang, and R. Ross, "Skeletal muscle mass and distribution in 468 men and women aged 18–88 yr," *Journal of applied physiology*, vol. 89, no. 1, pp. 81–88, 2000.

[16] S. B. Heymsfield, "Development of imaging methods to assess adiposity and metabolism," *International Journal of Obesity*, vol. 32, pp. S76–S82, 2008.

[17] W. T. Dixon, "Simple proton spectroscopic imaging.," *Radiology*, vol. 153, no. 1, pp. 189–194, 1984.

[18] B. H. Goodpaster, D. E. Kelley, F. L. Thaete, J. He, and R. Ross, "Skeletal muscle attenuation determined by computed tomography is associated with skeletal muscle lipid content," *Journal of applied physiology*, vol. 89, no. 1, pp. 104–110, 2000.

[19] D. M. Cutler and L. Sheiner, "Demographics and medical care spending: standard and non-standard effects," tech. rep., National bureau of economic research, 1998.

[20] B. H. Singer and K. G. Manton, "The effects of health changes on projections of health service needs for the elderly population of the united states," *Proceedings of the National Academy of Sciences*, vol. 95, no. 26, pp. 15618–15622, 1998.

[21] S. Orgiu, C. L. Lafortuna, F. Rastelli, and G. Rizzo, "Automatic segmentation of thigh mri to assess regional composition in young and old females," in *GNB Congress 2014, 25-27 June, Pavia*.

[22] C. Laforortuna, F. Rastelli, M. Caramenti, S. Orgius, P. Capodaglio, A. Falini, and G. Rizzo, "Muscle size, composition and architecture: effects on leg specific strength in obese older women," in *8th Fribourg Obesity Research Conference (FORC-2015), 10 settembre, Friburgo, Svizzera.*

[23] C. P. Rastelli, F and., M. Caramenti, C. Santovito, S. Orgiu, M. Cadioli, A. Falini, G. Rizzo, and L. Claudio, "Muscle strenght and architecture in obese older women," in *EUGMS Congress 2014, 17-19 September, Rotterdam, The Netherlands.*

[24] L. W. Goldman, "Principles of ct and ct technology," *Journal of nuclear medicine technology*, vol. 35, no. 3, pp. 115–128, 2007.

[25] A. C. Kak and M. Slaney, *Principles of computerized tomographic imaging*. SIAM, 2001.

[26] T. M. ROBINSON, *BASIC PRINCIPLES OF ULTRASOUND*, pp. 101–110. Dordrecht: Springer Netherlands, 2007.

[27] C. Westbrook and C. K. Roth, *MRI in Practice*. John Wiley & Sons, 2011.

[28] C. M. Prado and S. B. Heymsfield, "Lean tissue imaging: a new era for nutritional assessment and intervention," *Journal of Parenteral and Enteral Nutrition*, vol. 38, no. 8, pp. 940–953, 2014.

[29] C. L. Lafortuna, D. Tresoldi, and G. Rizzo, "Influence of body adiposity on structural characteristics of skeletal muscle in men and women," *Clinical physiology and functional imaging*, vol. 34, no. 1, pp. 47–55, 2014.

[30] B. H. Goodpaster, C. L. Carlson, M. Visser, D. E. Kelley, A. Scherzinger, T. B. Harris, E. Stamm, and A. B. Newman, "Attenuation of skeletal muscle and strength in the elderly: The health abc study," *Journal of Applied Physiology*, vol. 90, no. 6, pp. 2157–2165, 2001.

[31] R. Ross, "Advances in the application of imaging methods in applied and clinical physiology," *Acta diabetologica*, vol. 40, pp. s45–s50, 2003.

[32] J. Simoneau, S. Colberg, F. L. Thaete, and D. Kelley, "Skeletal muscle glycolytic and oxidative enzyme capacities are determinants of insulin sensitivity and muscle composition in obese women.," *The FASEB Journal*, vol. 9, no. 2, pp. 273–278, 1995.

[33] S. K. Gujar, S. Maheshwari, I. Björkman-Burtscher, and P. C. Sundgren, "Magnetic resonance spectroscopy," *Journal of neuro-ophthalmology*, vol. 25, no. 3, pp. 217–226, 2005.

[34] S. Deshmukh, T. Subhawong, J. A. Carrino, and L. Fayad, "Role of mr spectroscopy in musculoskeletal imaging," *The Indian journal of radiology & imaging*, vol. 24, no. 3, p. 210, 2014.

[35] C. P. Bernard, G. P. Liney, D. J. Manton, L. W. Turnbull, and C. M. Langton, "Comparison of fat quantification methods: a phantom study at 3.0 t," *Journal of magnetic resonance imaging*, vol. 27, no. 1, pp. 192–197, 2008.

[36] R. Sinha, S. Dufour, K. F. Petersen, V. LeBon, S. Enoksson, Y.-Z. Ma, M. Savoye, D. L. Rothman, G. I. Shulman, and S. Caprio, "Assessment of skeletal muscle triglyceride content by 1 h nuclear magnetic resonance spectroscopy in lean and obese adolescents," *Diabetes*, vol. 51, no. 4, pp. 1022–1027, 2002.

[37] H. Howald, C. Boesch, R. Kreis, S. Matter, R. Billeter, B. Essen-Gustavsson, and H. Hoppeler, "Content of intramyocellular lipids derived by electron microscopy, biochemical assays, and 1 h-mr spectroscopy," *Journal of Applied Physiology*, vol. 92, no. 6, pp. 2264–2272, 2002.

[38] L. S. Szczepaniak, E. E. Babcock, F. Schick, R. L. Dobbins, A. Garg, D. K. Burns, J. D. McGarry, and D. T. Stein, "Measurement of intracellular triglyceride stores by h spectroscopy: validation in vivo," *American Journal of Physiology-Endocrinology And Metabolism*, vol. 276, no. 5, pp. E977–E989, 1999.

[39] J. Ma, "Dixon techniques for water and fat imaging," *Journal of Magnetic Resonance Imaging*, vol. 28, no. 3, pp. 543–558, 2008.

[40] H. Eggers and P. Börnert, "Chemical shift encoding-based water–fat separation methods," *Journal of Magnetic Resonance Imaging*, vol. 40, no. 2, pp. 251–268, 2014.

[41] G. Glover and E. Schneider, "Three-point dixon technique for true water/fat decomposition with b0 inhomogeneity correction," *Magnetic resonance in medicine*, vol. 18, no. 2, pp. 371–383, 1991.

[42] J. Noble, S. Keevil, J. Totman, and G. Charles-Edwards, "In vitro and in vivo comparison of two-, three-and four-point dixon techniques for clinical intramuscular fat quantification at 3 t," *The British journal of radiology*, vol. 87, no. 1036, p. 20130761, 2014.

[43] M. A. Fischer, C. W. Pfirrmann, N. Espinosa, D. A. Raptis, and F. M. Buck, "Dixon-based mri for assessment of muscle-fat content in phantoms, healthy volunteers and patients with achillodynia: comparison to visual assessment of calf muscle quality," *European radiology*, vol. 24, no. 6, pp. 1366–1375, 2014.

[44] T. A. Wren, S. Bluml, L. Tseng-Ong, and V. Gilsanz, "Three-point technique of fat quantification of muscle tissue as a marker of disease progression in duchenne muscular dystrophy: preliminary study," *American Journal of Roentgenology*, vol. 190, no. 1, pp. W8–W12, 2008.

[45] H. H. Hu, Y. Li, T. R. Nagy, M. I. Goran, and K. S. Nayak, "Quantification of absolute fat mass by magnetic resonance imaging: a validation study against chemical analysis," *International journal of body composition research*, vol. 9, no. 3, p. 111, 2011.

[46] B. Guiu, J.-M. Petit, R. Loffroy, D. Ben Salem, S. Aho, D. Masson, P. Hillon, D. Krause, and J.-P. Cercueil, "Quantification of liver fat content: comparison of triple-echo chemical shift gradient-echo imaging and in vivo proton mr spectroscopy," *Radiology*, vol. 250, no. 1, pp. 95–102, 2009.

[47] M. Maas, E. M. Akkerman, H. W. Venema, J. Stoker, and G. J. Den Heeten, "Dixon quantitative chemical shift mri for bone marrow evaluation in the lumbar spine: a reproducibility study in healthy volunteers," *Journal of computer assisted tomography*, vol. 25, no. 5, pp. 691–697, 2001.

[48] R. L. Lieber and J. Friden, "Functional and clinical significance of skeletal muscle architecture," *Muscle & nerve*, vol. 23, no. 11, pp. 1647–1666, 2000.

[49] M. V. Narici, T. Binzoni, E. Hiltbrand, J. Fasel, F. Terrier, and P. Cerretelli, "In vivo human gastrocnemius architecture with changing joint angle at rest and during graded isometric contraction.," *The Journal of Physiology*, vol. 496, no. 1, pp. 287–297, 1996.

[50] D. Le Bihan, J.-F. Mangin, C. Poupon, C. A. Clark, S. Pappata, N. Molko, and H. Chabriat, "Diffusion tensor imaging: concepts and applications," *Journal of magnetic resonance imaging*, vol. 13, no. 4, pp. 534–546, 2001.

[51] J. Oudeman, A. J. Nederveen, G. J. Strijkers, M. Maas, P. R. Luijten, and M. Froeling, "Techniques and applications of skeletal muscle diffusion tensor imaging: a review," *Journal of Magnetic Resonance Imaging*, vol. 43, no. 4, pp. 773–788, 2016.

[52] B. M. Damon, Z. Ding, A. W. Anderson, A. S. Freyer, and J. C. Gore, "Validation of diffusion tensor mri-based muscle fiber tracking," *Magnetic resonance in medicine*, vol. 48, no. 1, pp. 97–104, 2002.

[53] J. Qi, N. J. Olsen, R. R. Price, J. A. Winston, and J. H. Park, "Diffusion-weighted imaging of inflammatory myopathies: Polymyositis and dermatomyositis," *Journal of Magnetic Resonance Imaging*, vol. 27, no. 1, pp. 212–217, 2008.

[54] G. Didier and F. Odette, *Encyclopedia of Biomaterials and Biomedical Engineering, Second Edition Edited Pages 956-967.* 2008.

[55] R. A. Meyer and B. M. Prior, "Functional magnetic resonance imaging of muscle," *Exerc Sport Sci Rev*, vol. 28, no. 2, pp. 89–92, 2000.

[56] B. M. Damon, M. C. Wadington, J. L. Hornberger, and D. A. Lansdown, "Absolute and relative contributions of bold effects to the muscle functional mri signal intensity time course: effect of exercise intensity," *Magnetic resonance in medicine*, vol. 58, no. 2, pp. 335–345, 2007.

[57] R. Kinugasa, Y. Kawakami, and T. Fukunaga, "Quantitative assessment of skeletal muscle activation using muscle functional mri," *Magnetic resonance imaging*, vol. 24, no. 5, pp. 639–644, 2006.

[58] M. Y. Endo, M. Kobayakawa, R. Kinugasa, S. Kuno, H. Akima, H. B. Rossiter, A. Miura, and Y. Fukuba, "Thigh muscle activation distribution and pulmonary vo 2 kinetics during moderate, heavy, and very heavy intensity cycling exercise in humans," *American Journal of Physiology-Regulatory, Integrative and Comparative Physiology*, vol. 293, no. 2, pp. R812–R820, 2007.

[59] B. M. Damon, D. M. Wigmore, Z. Ding, J. C. Gore, and J. A. Kent-Braun, "Cluster analysis of muscle functional mri data," *Journal of applied physiology*, vol. 95, no. 3, pp. 1287–1296, 2003.

[60] W. Shen, Z. Wang, M. Punyanita, J. Lei, A. Sinav, J. G. Kral, C. Imielinska, R. Ross, and S. B. Heymsfield, "Adipose tissue quantification by imaging methods: a proposed classification," *Obesity*, vol. 11, no. 1, pp. 5–16, 2003.

[61] G. Brunner, V. Nambi, E. Yang, A. Kumar, S. S. Virani, P. Kougias, D. Shah, A. Lumsden, C. M. Ballantyne, and J. D. Morrisett, "Automatic quantification of muscle volumes in magnetic resonance imaging scans of the lower extremities," *Magnetic resonance imaging*, vol. 29, no. 8, pp. 1065–1075, 2011.

[62] B. J. Broderick, S. Dessus, P. A. Grace, and G. ÓLaighin, "Technique for the computation of lower leg muscle bulk from magnetic resonance images," *Medical engineering & physics*, vol. 32, no. 8, pp. 926–933, 2010.

[63] L. Urricelqui, A. Malanda, and A. Villanueva, "Automatic segmentation of thigh magnetic resonance images," in *WASET Congress*, vol. 58, p. 979, 2009.

[64] V. Barra and J.-Y. Boire, "Segmentation of fat and muscle from mr images of the thigh by a possibilistic clustering algorithm," *Computer methods and programs in biomedicine*, vol. 68, no. 3, pp. 185–193, 2002.

[65] S. Makrogiannis, S. Serai, K. W. Fishbein, C. Schreiber, L. Ferrucci, and R. G. Spencer, "Automated quantification of muscle and fat in the thigh from water-, fat-, and nonsuppressed mr images," *Journal of Magnetic Resonance Imaging*, vol. 35, no. 5, pp. 1152–1161, 2012.

[66] A. Valentinitsch, D. C Karampinos, H. Alizai, K. Subburaj, D. Kumar, T. M Link, and S. Majumdar, "Automated unsupervised multi-parametric classification of adipose tissue depots in skeletal muscle," *Journal of Magnetic Resonance Imaging*, vol. 37, no. 4, pp. 917–927, 2013.

[67] V. Positano, T. Christiansen, M. F. Santarelli, S. Ringgaard, L. Landini, and A. Gastaldelli, "Accurate segmentation of subcutaneous and intermuscular adipose tissue from mr images of the thigh," *Journal of Magnetic Resonance Imaging*, vol. 29, no. 3, pp. 677–684, 2009.

[68] Z. Hou, "A review on mr image intensity inhomogeneity correction," *International Journal of Biomedical Imaging*, vol. 2006, 2006.

[69] O. Salvado, C. Hillenbrand, S. Zhang, and D. L. Wilson, "Method to correct intensity inhomogeneity in mr images for atherosclerosis characterization," *IEEE Transactions on Medical Imaging*, vol. 25, no. 5, pp. 539–552, 2006.

[70] J. C. Bezdek, R. Ehrlich, and W. Full, "Fcm: The fuzzy c-means clustering algorithm," *Computers & Geosciences*, vol. 10, no. 2-3, pp. 191–203, 1984.

[71] M. Kass, A. Witkin, and D. Terzopoulos, "Snakes: Active contour models," *International journal of computer vision*, vol. 1, no. 4, pp. 321–331, 1988.

[72] T. Heimann, B. Van Ginneken, M. A. Styner, Y. Arzhaeva, V. Aurich, C. Bauer, A. Beck, C. Becker, R. Beichel, G. Bekes, *et al.*, "Comparison and evaluation of methods for liver segmentation from ct datasets," *IEEE transactions on medical imaging*, vol. 28, no. 8, pp. 1251–1265, 2009.

[73] C. R. Maurer, R. Qi, and V. Raghavan, "A linear time algorithm for computing exact euclidean distance transforms of binary images in arbitrary dimensions," *IEEE Transactions on Pattern Analysis and Machine Intelligence*, vol. 25, no. 2, pp. 265–270, 2003.

[74] J. Rybak, A. Kuß, H. Lamecker, S. Zachow, H.-C. Hege, M. Lienhard, J. Singer, K. Neubert, and R. Menzel, "The digital bee brain: integrating and managing neurons in a common 3d reference system," *Frontiers in systems neuroscience*, vol. 4, 2010.

[75] K. Segal, M. Van Loan, P. Fitzgerald, J. Hodgdon, and T. B. Van Itallie, "Lean body mass estimation by bioelectrical impedance analysis: a four-site cross-validation study.," *The American journal of clinical nutrition*, vol. 47, no. 1, pp. 7–14, 1988.

[76] D. S. Gray, G. A. Bray, N. Gemayel, and K. Kaplan, "Effect of obesity on bioelectrical impedance.," *The American journal of clinical nutrition*, vol. 50, no. 2, pp. 255–260, 1989.

[77] M. V. Narici, C. Maganaris, and N. Reeves, "Myotendinous alterations and effects of resistive loading in old age," *Scandinavian journal of medicine & science in sports*, vol. 15, no. 6, pp. 392–401, 2005.

[78] J. M. Thom, C. I. Morse, K. M. Birch, and M. V. Narici, "Influence of muscle architecture on the torque and power–velocity characteristics of young and elderly men," *European journal of applied physiology*, vol. 100, no. 5, pp. 613–619, 2007.

[79] M. V. Narici, C. N. Maganaris, N. D. Reeves, and P. Capodaglio, "Effect of aging on human muscle architecture," *Journal of applied physiology*, vol. 95, no. 6, pp. 2229–2234, 2003.

[80] C. Suetta, L. G. Hvid, L. Justesen, U. Christensen, K. Neergaard, L. Simonsen, N. Ortenblad, S. P. Magnusson, M. Kjaer, and P. Aagaard, "Effects of aging on human skeletal muscle after immobilization and retraining," *Journal of Applied Physiology*, vol. 107, no. 4, pp. 1172–1180, 2009.

[81] P. Aagaard, J. L. Andersen, P. Dyhre-Poulsen, A.-M. Leffers, A. Wagner, S. P. Magnusson, J. Halkjær-Kristensen, and E. B. Simonsen, "A mechanism for increased contractile strength of human pennate muscle in response to strength training: changes in muscle architecture," *The journal of physiology*, vol. 534, no. 2, pp. 613–623, 2001.

[82] A. J. Blazevich, D. Cannavan, D. R. Coleman, and S. Horne, "Influence of concentric and eccentric resistance training on architectural adaptation in human quadriceps muscles," *Journal of Applied Physiology*, vol. 103, no. 5, pp. 1565–1575, 2007.

[83] O. R. Seynnes, M. de Boer, and M. V. Narici, "Early skeletal muscle hypertrophy and architectural changes in response to high-intensity resistance training," *Journal of applied physiology*, vol. 102, no. 1, pp. 368–373, 2007.

[84] D. Tomlinson, R. Erskine, K. Winwood, C. Morse, and G. Onambélé, "The impact of obesity on skeletal muscle architecture in untrained young vs. old women," *Journal of anatomy*, vol. 225, no. 6, pp. 675–684, 2014.

[85] R. M. Erskine, D. A. Jones, C. N. Maganaris, and H. Degens, "In vivo specific tension of the human quadriceps femoris muscle," *European journal of applied physiology*, vol. 106, no. 6, p. 827, 2009.

[86] T. D. O'Brien, N. D. Reeves, V. Baltzopoulos, D. A. Jones, and C. N. Maganaris, "Muscle–tendon structure and dimensions in adults and children," *Journal of anatomy*, vol. 216, no. 5, pp. 631–642, 2010.

[87] M. Hulens, G. Vansant, R. Lysens, A. Claessens, E. Muls, and S. Brumagne, "Study of differences in peripheral muscle strength of lean versus obese women: an allometric approach," *International journal of obesity*, vol. 25, no. 5, p. 676, 2001.

[88] N. A. Maffiuletti, S. Ratel, A. Sartorio, and V. Martin, "The impact of obesity on in vivo human skeletal muscle function," *Current Obesity Reports*, vol. 2, no. 3, pp. 251–260, 2013.

[89] A. B. Newman, C. L. Haggerty, B. Goodpaster, T. Harris, S. Kritchevsky, M. Nevitt, T. P. Miles, and M. Visser, "Strength and muscle quality in a well-functioning cohort of older adults: The health, aging and body composition study," *Journal of the American Geriatrics Society*, vol. 51, no. 3, pp. 323–330, 2003.

[90] S. Ikegawa, K. Funato, N. Tsunoda, H. Kanehisa, T. Fukunaga, and Y. Kawakami, "Muscle force per cross-sectional area is inversely related with pennation angle in strength trained athletes," *The Journal of Strength & Conditioning Research*, vol. 22, no. 1, pp. 128–131, 2008.

[91] A. J. Blazevich, "Effects of physical training and detraining, immobilisation, growth and aging on human fascicle geometry," *Sports Medicine*, vol. 36, no. 12, pp. 1003–1017, 2006.

[92] T. Wakahara, H. Kanehisa, Y. Kawakami, T. Fukunaga, and T. Yanai, "Relationship between muscle architecture and joint performance during concentric contractions in humans," *Journal of applied biomechanics*, vol. 29, no. 4, pp. 405–412, 2013.